Submarine Design Optimization Using Boundary Layer Control

by

Christopher L. Warren

B.S.M.E. North Carolina State University, 1987

Submitted to the Department of Ocean Engineering
and the Department of Mechanical Engineering
in Partial Fulfillment of the Requirements for the Degrees of

Naval Engineer
and
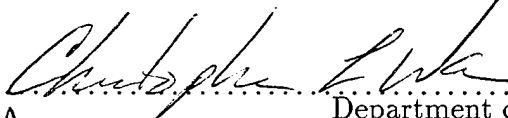Master of Science in Mechanical Engineering

at the
MASSACHUSETTS INSTITUTE OF TECHNOLOGY
June 1997

©1997 Christopher L. Warren. All rights reserved.

The author hereby grants to MIT permission to reproduce
and to distribute publicly paper and electronic
copies of this thesis document in whole or in part.
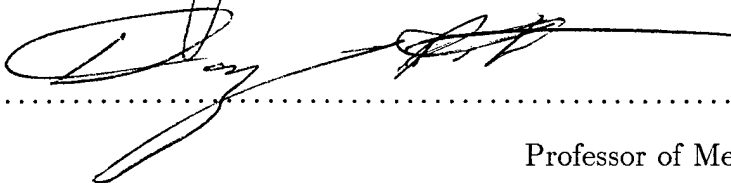
Signature of Author ....
Department of Ocean Engineering
May 9, 1997

Certified by ....
Justin E. Kerwin
Professor of Naval Architecture
Thesis Supervisor
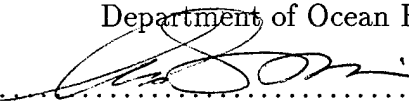
Certified by ....
Douglas Hart
Professor of Mechanical Engineering
Thesis Supervisor

Accepted by ....
Kim Vandiver
Chairman, Committee on Graduate Students
Department of Ocean Engineering

Accepted by ....
Ain Ants Sonin
Chairman, Committee on Graduate Students
Department of Mechanical Engineering

19970703 074

DTIC QUALITY INSPECTED 1

Submarine Design Optimization Using Boundary Layer Control

by

Christopher L. Warren

Submitted to the Department of Ocean Engineering
and
the Department of Mechanical Engineering
on May 9, 1997, in partial fulfillment of the
requirements for the degrees of
Naval Engineer
and
Master of Science in Mechanical Engineering

Abstract

Several hull designs are studied with parametric based volume and area estimates to obtain preliminary hull forms. The volume and area study includes the effects of technologies which manifest themselves in the parametric study through stack length requirements. Subsequently, the hull forms are studied using a Reynolds Averaged Navier Stokes analysis coupled with a vortex lattice propeller design code. Optimization is done through boundary layer control analysis and through studies on the effect of blade loading magnitudes and profiles. Several hull form afterbody shapes are studied to improve the powering characteristics of a full stern submarine. The hydrodynamic analysis includes the total contribution of the rotor, stator, duct, the body hull form and appendages on the submarine drag. Corrections are developed and applied to extrapolate the model scale hydrodynamic results to a full scale submarine. The end result gives a speed of the hull form which is used to optimize the overall submarine. The basic measure of the overall effect of stern taper is the maximum speed of the submarine while keeping the same shaft horse power propulsion plant, the same volume and the same area requirements. The hydrodynamic powering efficiency is discussed and evaluated using a power coefficient. The resulting designs have marked differences in length but similar displacements and similar maximum speeds. The results promise great potential for the full stern submarine.

Thesis Supervisor: Justin E. Kerwin
Title: Professor of Naval Architecture

Thesis Supervisor: Douglas Hart
Title: Professor of Mechanical Engineering

Acknowledgments

My time at MIT was rich with learning, personal revelations, and meeting new friends. I have gained the insider's perspective on the scientific community and the fundamental appreciation of the need to support scientific research. By studying both the academic material and the broader ship design issues, I have gained a better understanding of the present and future needs of the Navy.

Many people helped to make my time successful and rewarding. I offer my sincerest gratitude and warmest thank you.

Foremost, I thank my family. My wife, who is my dearest friend, shares my triumphs and my failures. Her steadfast, genuine support inspires me to study the areas in the breath and the depth that I chose without the guilt or dilemma that I must chose between the work I enjoy and the family I love. I thank my children, Britney and Chad, for reminding me that life flourishes outside of the stone walls of MIT.

I thank the U.S. Navy for providing me a great career with challenging assignments and rewarding opportunities. I thank the Navy Academic Office, Capt. Brown, Lcdr Welsh, and Richard, for handling the routine things to allow me to focus on the task at hand. I especially thank Prof. Welsh for his guidance and mentorship.

I thank the Propnuts group for enduring support and motivation. Without this group, my experiences would have sorely missed the fundamental academia of MIT.

Not least, I thank my 13A counterparts. Our spontaneous fraternity provided the needed checks and balances to make the experiences both bearable and enjoyable.

Contents

List of Figures

List of Tables

Nomenclature

Mathematic Notation

C_P $\dfrac{2\pi n Q}{\frac{1}{2}\rho V_S^3 A_B}$ Power Coefficient

C_Q $\dfrac{Q}{\frac{1}{2}\rho V_s^2 \pi R^3}$ torque coefficient based on ship speed

C_T $\dfrac{T}{\frac{1}{2}\rho V_s^2 \pi R^2}$ thrust coefficient based on ship speed

C_D $\dfrac{Drag}{\frac{1}{2}\rho V_s^2 \pi R^2}$ thrust coefficient based on ship speed

G $\dfrac{\Gamma}{2\pi R V_s}$ non-dimensional circulation

J_a $\dfrac{V_a}{nD}$ advance coefficient based on speed of advance

J_s $\dfrac{V_s}{nD}$ advance coefficient based on ship speed

K_Q $\dfrac{Q}{\rho n^2 D^5}$ torque coefficient based on rps

K_T $\dfrac{T}{\rho n^2 D^4}$ thrust coefficient based on rps

Other Nomenclature

A_B		frontal area of the axisymmetric body
C_m		foefficient of mass flow
D		propeller diameter
D_B		body diameter
n		propeller revolutions per second
Q		propeller torque
R		propeller radius
$\Re$	$\frac{ul}{\nu}$	Reynolds number
R_T		unpropelled resistance
r/R		local radius
$(1-t)$		thrust deduction factor
T		propeller thrust
V_a	$V_s(1-w)$	velocity of advance
V_s		ship speed
w		Taylor wake fraction
x/L		local axial position
$\mathcal{Z}$		number of propeller blades
Γ		dimensional circulation
η_r		relative rotative efficiency
η_s		shaft efficiency
ν		kinematic viscosity of fluid
ρ		density of fluid

Abbreviations

ER	Engine Room
RANS	Reynolds-averaged Navier-Stokes (flow solver)
EHP	Effective Horsepower
LCG	Longitudinal Center of Gravity
SHP	Shaft Horsepower
PC	Propulsive Coefficient
PWR	Pressurized Water Reactor

Chapter 1

Introduction

1.1 Purpose of Thesis

The history of submarine design has lead to many improvements. From the earliest submarine, the Holland, to the newest attack submarine, advances in submarine technology usually proceed in methodical steps. Some revolutionary changes include the teardrop hull form of the Albacore and the advent of the nuclear age with the Nautilus [4]. Perhaps the next revolutionary change centers around the full stern hull form with an integrated propulsor.

Traditional submarines have their machinery weights located relatively aft to provide propulsion. A conflicting requirement to this is the necessity to taper the stern to prevent separation near the propulsor. A bridge in these two requirements may be the use of the full stern hull form. By maintaining a fuller stern further aft, the resulting hull form will gain a considerable amount of arrangeable volume. Thus, it is possible to move the machinery aft and, thereby, shorten the overall length of the submarine. With a shorter hull form and the same installed shaft horse power, the submarine may be able to exceed the speed of a conventional designed tapered stern. This thesis examines the issues surrounding the full stern design compromises.

1.2 Submarine Design Methods

Stack length describes the requirement that machinery must lie sequentially along the longitudinal axis of the submarine. Parametric based estimates use thumb rules to relate some known inputs to the size of the submarine. Some common inputs include: crew size, number of days underway, number of torpedos, etc. The parametric estimates can also include stack length considerations by requiring the most limiting of a specified length of a compartment or a minimum compartment volume.

One method to study the feasibility of a new submarine design uses parametric base estimates of area, volume and stack length. A second method uses parametric based estimates of weight. In the end, a submarine design must balance weight and volume such that the end product is neutrally buoyant. This study considers both volume and weight to use the "best" estimates of each methodology.

1.3 Full Stern Verses Conventional Taper

The term "taper" refers to the shape of the afterbody as it narrows down from a maximum hull diameter to the diameter necessary for smooth transition into the propeller regime. Traditional taper designs reach a tailcone half angle of no more than about 20 degrees. By limiting the taper transition to a small amount, fluid separation from the hull is avoided.

In a conventional design, the hull taper transitions from the maximum diameter to the propeller entrance in a length of 2 to 3 hull diameters. A more unconventional design, investigated in this thesis and labeled a "full stern", has a much larger transition rate near the propeller. The full stern narrows from the maximum hull diameter to the propeller entrance in a longitudinal distance on the order of one hull diameter. Using a form of boundary layer control, fluid separation is prevented by accelerating the boundary layer into the annular ring at the entrance to the duct.

One disadvantage to a full stern submarine is the possible loss of propulsor ef-

ficiency due to increased frictional and form drag when flow enters the duct. This apparent disadvantage is studied further in this thesis. While the efficiency may decrease, the submarine may actually have a faster maximum speed due to the shorter hull form and better length to diameter ratio.

Chapter 2

Design Process

2.1 Baseline Concept Design

The baseline submarine, used for arrangements comparisons, is a "conventional" submarine design. The baseline is balanced using parametric relationships originating in a course taught by Capt. (ret.) Harry Jackson entitled "Submarine Design Trends." The majority of the relationships are for submarines with 10,000 shaft horsepower (SHP) or more. The established baseline falls below the range of some of these parametrics. Consequently, in developing the baseline, comparative naval architecture trends are used to extend the various relationships to a smaller submarine and correctly size those items which are not easily scaled [26].

The baseline, shown in Figure 2-1, uses existing submarine technologies and near-future technologies that could be applied to the next generation submarine. Developed to meet the requirements of reference [11], the baseline has a crew of 40 persons, four torpedo tubes with space and weight for 20 torpedoes and a diving depth of 1000 feet. The baseline has allocated space and weight of 400 ft^2 and 80 $ltons$ to support a reconfigurable mission module. The module size meets the maximum for a variety of missions. Of the missions considered, the maximum space is required to support one platoon of Special Operating Forces plus their support equipment. The maximum weight payload is needed in support of anti-submarine warfare to carry a large torpedo payload of 30 torpedoes and handling gear beyond the organic capability of
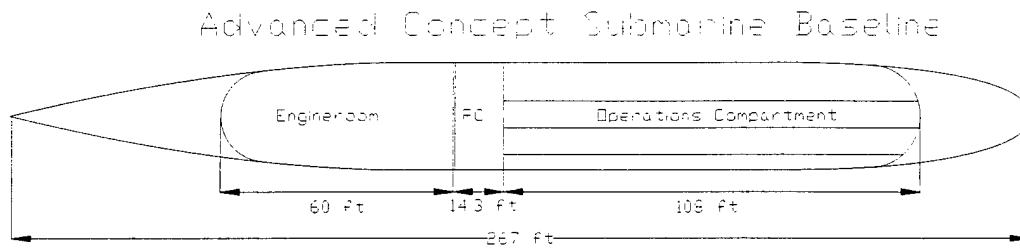
Figure 2-1: Advanced Concept Submarine Baseline

Characteristics	Baseline
Submerged Displacement	3221 *lton*
Speed (*kts*)	21.1
Installed *SHP*	5500
Depth (*ft*)	1000
Crew	40
Endurance Stores	45
Number of Weapons	20

Table 2.1: Baseline Characteristics Verses the Goal and Threshold Ship Characteristics

20 torpedoes.

The propulsion plant of the baseline submarine is a 5500 SHP Pressurized Water Reactor (PWR) with a steam system to turn steam turbine generators and steam main engines. Power from the main engines transmits through reduction gears, a thrust bearing, coupling, shaft seals, etc., to the propeller. The stack length of all of these components is estimated to be 60 feet. The estimated stack length is based on scaled interpolation from various sources [8], [12], [14], [25]. Figure 2-2 contains the estimated stack lengths for the baseline submarine. Table 2.1 provides a summary of the baseline design.

2.2 Full Stern Verses a Tapered Stern for a Submarine

A full stern design gives considerable flexibility in the submarine internal and external arrangements. The fuller stern provides added buoyancy. This buoyancy allows the

14
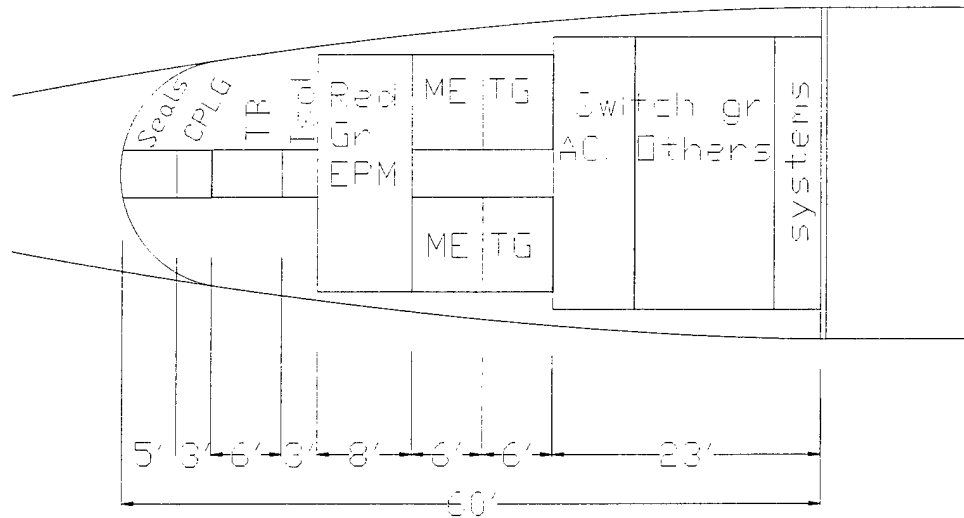
Figure 2-2: Baseline submarine engine room stack length based on scaled interpolation to 5500 SHP.

propulsion equipment to be shifted aft, where the limit may become equipment stack length, and thus provide more forward space for command and control functions. Recent studies have shown that a full stern reduces the submarine length by 5 to 18 percent while keeping the same equipment and weights within the submarine envelope [24], [30]. Additionally, the shorter submarine has a length to diameter ratio closer to the optimal of six to one [4].

A typical tapered submarine propulsive coefficient (PC) ranges from 0.7 to 0.9. There exist a wide range of estimates from various authors [4], [13], [23]. Thurston and Evanbar provide a fundamental discussion on the propulsive efficiency of a body of revolution and give insight as to why there exist a wide variation [29]. By assuming that the traditional naval architecture formulas for a tapered hull apply to a full stern (i.e. ignore the separation), a PC can be used to predict the speed of a full stern submarine during early parametric studies. The propulsive coefficient decreases from about 0.9 to about 0.8 when a full stern is added to a submarine [23]. The PC, defined by $PC = \frac{EHP}{SHP}$, is actually greater than 1.0 for a full stern. Section 4.3.4 elaborates.
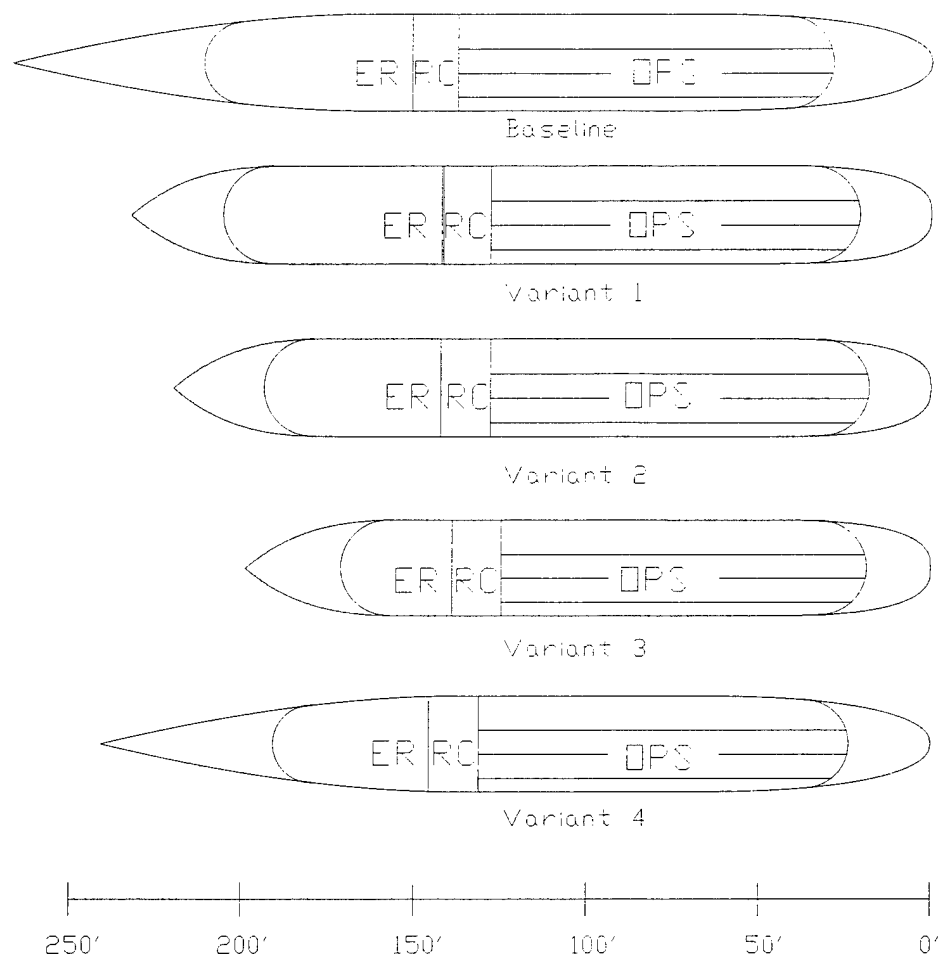
Figure 2-3: Profile comparison of the baseline and all variants used in the arrangements study.

2.3 Comparison of Arrangements

The baseline and all the variants are balanced with the principle characteristics given in Table 2.2. A profile comparison of the baseline and all the variants is shown in Figure 2-3.

Several key features are held constant between the baseline and the variants to provide a meaningful comparison. Specifically, the shaft horsepower is maintained at 5500 SHP and the hull diameter is maintained at 28 ft. The Operations Compart-

	Baseline	Variant 1	Variant 2	Variant 3	Variant 4
LBP (ft)	267	232	220	199	244
Sub. Disp. ($ltons$)	3221	3331	3125	2781	2837
SHP (hp)	5500	5500	5500	5500	5500
D (ft)	28	28	28	28	28
L/D	9.5	8.3	7.9	7.1	8.7
Volume (ft^3)	121,200	125,300	117,600	104,700	106,800
Wet. Surf. (ft^2)	19,200	18,750	17,640	15,140	17,800
Vol/ Wet Surf	6.31	6.68	6.67	6.91	6.00
ER length (ft)	60	60	48.7	32.5	48
ER volume (ft^3)	31,040	34,050	27,080	17,080	22,340
Propulsive Coef.*	0.842	0.81	0.81	0.81	0.834
Estimated Max speed (kts)	21.1	20.9	21.2	21.8	21.6
Stern Shape	Tapered	Full Stern	Full Stern	Full Stern	Tapered
Features	PWR	PWR	PWR	PWR	PWR
			Elect Dr	Elect Dr	Elect Dr
				Ext Motor	Ext Motor

* Note: The *PC* for all full stern variants is a best estimate value which will allow
the traditional formulas to give a reasonable estimate of speed. The *PC* for the other
variants is a calculated estimate from parametric equations.

Table 2.2: Principle Characteristics of Each Variant

ment area and weights, as well as the Reactor Compartment volume, are the same in
the baseline and all variants.

When a methodical comparison between full stern and tapered stern submarines is
carefully done, several difficulties present themselves. Foremost, a comparison based
on volume alone is inaccurate. In other words, the full stern with equal volume as a
tapered stern can not be arranged internally with the same PWR mechanical drive
power plant due to stack length requirements. Accordingly, variant 1 requires a ER
stack length of 60 feet which results in excess ER volume due to the full stern char-
acteristic. To design a competitive full stern submarine that is physically realizable,
technologies to reduce the stack length must be included in the design. Consequently,
this study considers the hull form (full stern or tapered) and various integral tech-
nologies. These considerations lead to the development of variants 1 through 4.

Variant 1 through 3 have the same hull form profile characteristics except for the
parallel mid-body length. A propulsive coefficient of 0.81 is assumed as the value
for the full stern submarine. The same *PC* is used in all full stern variants so that

the changes in maximum speed represent the variation due to the decreased wetted surface area and decreased form drag as the parallel mid-body is reduced. The PC does not represent the traditional definition of $PC = \dfrac{EHP}{SHP}$. Instead, these early parametric studies use the PC as a number which will allow the traditional formulas to give a reasonable estimate of speed. Section 4.3.4 elaborates.

2.4 Variant Descriptions

2.4.1 Variant 1 – PWR and Full Stern

Variant 1 has the same stack length in the ER as the baseline; however, the volume is re-shaped into a fuller stern and bow. The Operations Compartment (OPS) length is essentially unchanged. The overall length is reduced by 35 feet, due to the finely shaped aft ballast tanks and external items of the baseline being placed in the fuller hull. The surface displacement remains about the same. The wetted surface area decreases by 2% which reduces the frictional drag. At the same time, the PC decreases due to a less efficient propulsor resulting in a decrease in maximum speed of 0.2 knots.

2.4.2 Variant 2 – PWR, Full Stern and Electric Drive

Instead of a mechanical drive system as considered in the baseline, this variant uses an electric drive system. The advantage is a reduction in stack length from 60 feet to 48 feet and in required volume by 12% based on extrapolations derived from papers by Thomas Dade and Jeffery Dutton [8], [12].

Figure 2-4 contains the typical stack length assumed for this variant. Both the stack length and volume constraints are reached at essentially the same time; the volume constraint is most limiting and drives the engine room length to be 48.7 feet. The changes made to this variant shorten the baseline by 47 feet and represent a technically feasible engine room layout.
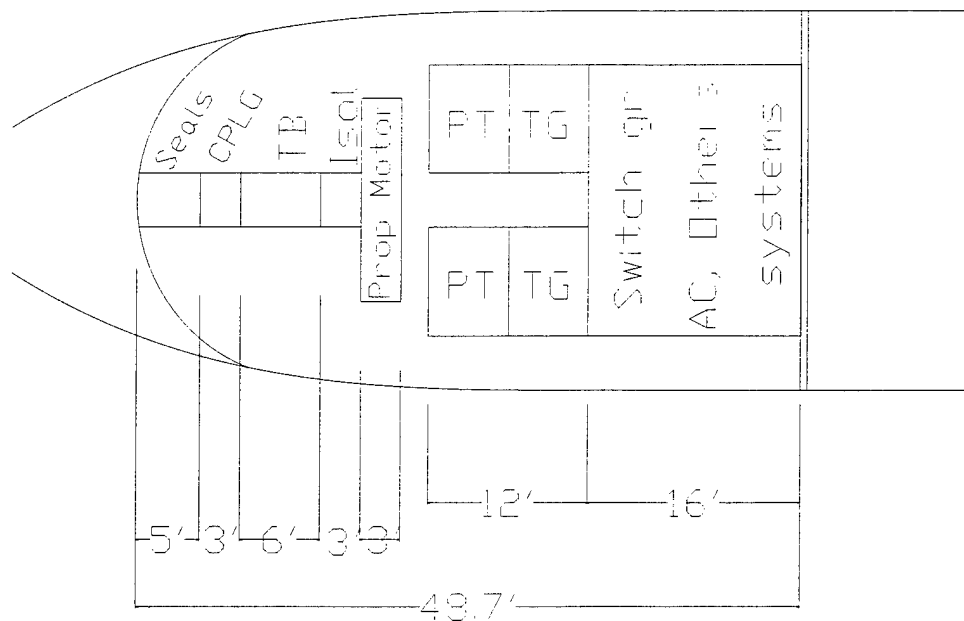
Figure 2-4: Electric Drive Typical Stack Length used for Variant 2

2.4.3 Variant 3 – PWR, Full Stern, and External Electric Drive

This variant takes variant 2 and places the drive train exterior to the pressure hull. It is envisioned that the propeller is actually a permanent magnet rotor and the mount and/or duct is a motor stator [1]. Accordingly, the drive train stack length due to shaft line components is completely eliminated. However, the free flood percentage of envelope displacement is roughly the same. The external drive motor technology has been recently demonstrated and is available for incorporation into a future submarine [9].

The savings in volume and stack length are roughly estimated using previous papers that compare and contrast engine room arrangements such as Dade and Dutton. The stack length is estimated to be two-thirds of the original engine room length which compares well with the removal of the shaft line components from the stack length in

the original engine room. As in variant 2, this variant represents a technically feasible engine room layout.

2.4.4 Variant 4 – PWR, Tapered Stern, and External Electric Drive

This variant answers the question: "If the new technologies are placed in a taper hull, how would it compare to the best full stern hull?" The reason that this variant is less favorable than the equivalent full stern variant is its lack of buoyancy aft. With the high power density afforded external electric drive, the propulsion plant occupies relatively little volume. And consequently, the submarine tends to sink by the stern. Trim lead can be used to balance the longitudinal trim of the submarine, however, in this power dense variant, the lead needs to be located forward of the bow unless buoyancy is added aft to support the power plant. To bring the variant to a balance condition, the engine room volume is increased until ample buoyancy supports the power plant and allows reasonable placement of the lead within the hull envelope.

Figure 2-5 shows the variation in some submarine attributes as the engine room volume is increased to bring the placement of the lead within the hull envelope. The increased volume aft increases the submarine displacement and increases the length beyond that needed if longitudinal balance is not an issue. Accordingly, the maximum speed is less than what could be achieve with a smaller volume. Compared to Variant 3, this variant's displacement is 56 *ltons* greater, length is 45 feet longer and maximum speed 0.2 knots lower.

2.5 Conclusion of Full Stern Arrangements Study

In general, the stack length limits a full stern submarine such that all of the advantages of a full stern design are not realizable without reducing the traditional stack length of a propulsion system. Second, the submarine propulsion system and its power density plays a significant role in assessing the benefits of a full stern design. Third, the full stern design compliments an electric drive submarine, particularly, if the submarine
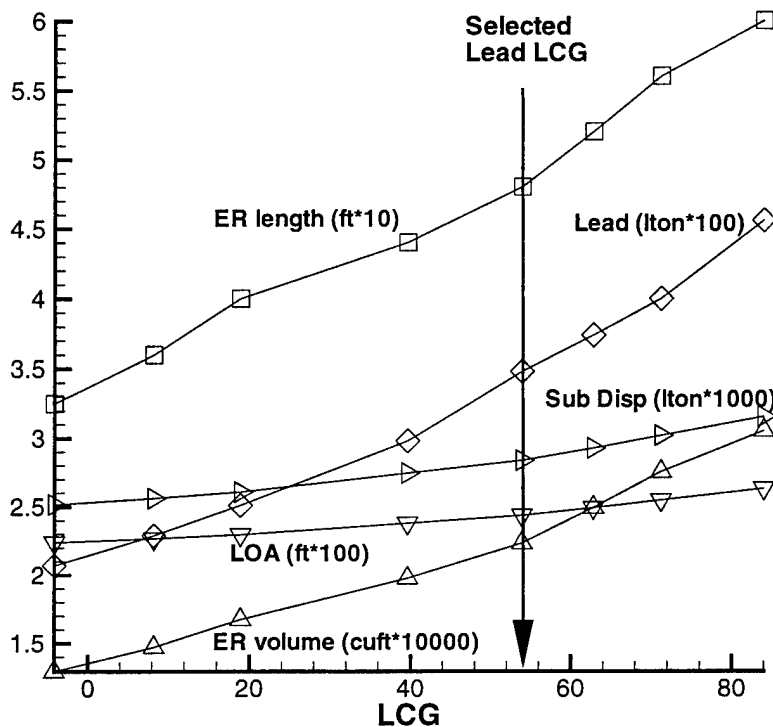
Figure 2-5: The bow is located at 0 *ft*, increasing *x* moves aft. The engine room volume determines the *LCG* of the lead. As engine room volume is increased, the aft buoyancy is increased and the *LCG* of the lead can be slid aft. The amount of lead also increases when engine room volume is increased since the submarine must submerge.

has external electric drive.

A profile comparison of Variant 3 and 4 can be seen in Figure 2-3. The full stern variant is 45 feet shorter and 56 *lton* lighter. The 22 knot speed of the two variant's is essentially the same. Each variant has unique features. Variant 3 has a full stern with its challenges in propulsor design and external electric drive. Variant 4 has more typical challenges of current designs with the added challenges of external electric drive. Using parametric estimates for the maximum speed, neither variant clearly stands out as the best submarine design.

More detailed hydrodynamic analysis will be done on Variant 3 and 4 in order to more accurately quantify their powering characteristics and to discover some useful

quantities by which quantitative comparisons can be made. It should be noted that Variants 3 and 4 all have the same technologies within their respective hull envelopes. As a result, performance differences represent the effects of the basic hull form differences. The particular power plant technologies used are inconsequential as long as the power plant technologies eliminate stack length.

Chapter 3

Lifting Surface / RANS Optimization

3.1 Parametric Studies

To evaluate the hydrodynamic characteristics, a preliminary design study is necessary. The preferred level of detail is a lifting line model of the propeller with a quasi-empirical estimate of the viscous effects on the body. One tool available at MIT is the Propeller Lifting Line (PLL) [7]. This code approximates the downstream helical wake as cylindrical and does not model the highly contracting wake expected in a full stern design. This difficulty lead to the Ducted Propeller Lifting Line (DPLL) [27]. While this code specifically models the contracting wake, it does not capture the full viscous nature of the inflow to the propulsor. Work is underway to improve DPLL modeling for a full stern bodies [28].

The issues above lead to the use of a Reynolds Averaged Navier Stokes (RANS) code to model the viscous nature of the inflow which was coupled with a vortex lattice Propeller Blade Design (PBD) code to model the propeller influence. The procedure commonly annotated as lifting surface / RANS coupling is discussed is several references [18], [2].

3.2 Lifting Surface / RANS Evaluation of Sirenian

In parallel with the arrangement study, a notional full stern body was developed to provide a starting basis for future iterations and improvements. The notional full stern body is designated *Sirenian*. It does not represent an optimal design in any respects. The Sirenian provides a starting basis to explore possible changes which may improve the powering characteristics.

3.2.1 Physical Geometry

The Sirenian has a total body length of 11.9 and a body radius of 1.0. The bow is elliptical to $x/L = 3.0$, parallel midbody from 3.0 to 8.9, then two cubic polynomials to close the body. The body offset equations are given in equations 3.1 through 3.4. The design Reynolds number for the RANS computations is 268829 based on body radius. The duct chord is 1.15 with thickness to chord (t/c) of 0.08 and camber to chord (f/c) of -0.02 at a 10 degree angle of attack. The trailing edge is located a $x/L = 11.57381821$ and $r/R = 0.70211869$. The duct thickness and camber distribution are shown in Figure 3-1.

Nose - Ellipse, $X = 0.0...3.0$

$$R = \frac{\sqrt{2.250 - (1.5 - X0.5)^2}}{\sqrt{2.25}} \tag{3.1}$$

Midbody - Cylinder, $X = 3.0...8.9$

$$R = 1.0 \tag{3.2}$$

Stern - Cubic Polynomial, $X = 8.9...11.47937081, H = (X - 8.9)$

$$R = 0.077216975H^3 - 0.3243113H^2 - 0.018737882H + 1.0 \tag{3.3}$$

Closure - Cubic Polynomial, $X = 11.47937081...11.899917$

$$R = -1.47967903X^3 + 51.257933X^2 - 592.00706X + 2279.7425 \tag{3.4}$$
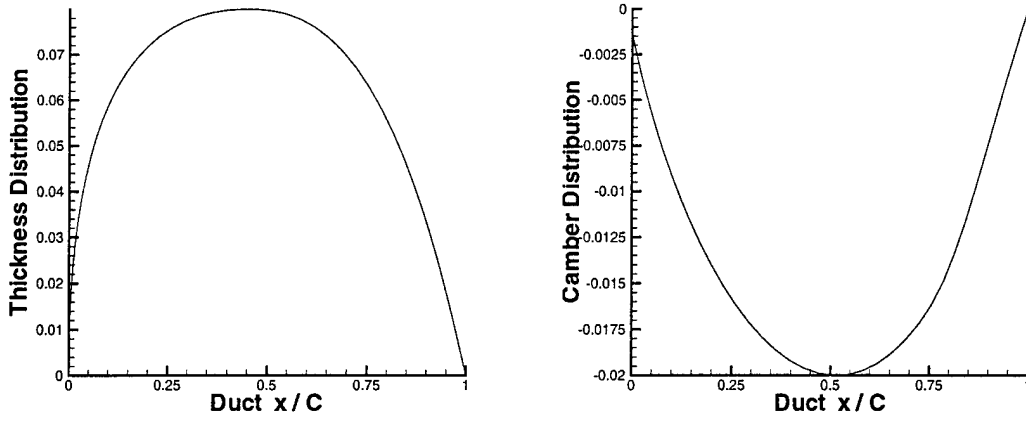
Figure 3-1: Duct thickness and camber distributions.

The stator has 11 blades with the leading edge tip at $x/L = 10.4948$ and $r/R = 0.857911$. The rotor has 6 blades with its leading edge tip at $x/L = 11.0854$ and $r/R = 0.719517$. There is no gap between the blades and the duct. The design J_s is 1.52.

3.2.2 RANS Grid

The RANS grid is constructed using INMESH code [5] and is shown in Figure 3-2. The RANS code used for this analysis is DTNSA, the axisymmetric version of the David Taylor Navier-Stokes codes developed by Gorski [16]. This code is formulated with the full Reynolds Averaged Navier Stokes equations.

The RANS grid is created with nearly constant spacing of the first cell off of the body in the normal directions $(y+)$. In order to capture the viscous sublayer of the boundary layer profile, a $y+$ between 1 and 4 is needed. The $y+$ parameter is a function of Reynolds number, which changes along the length of the body. For all bodies used throughout this thesis, a $y+$ of 1 to 4 is maintained along the entire body length to accurately capture the flow dynamics.
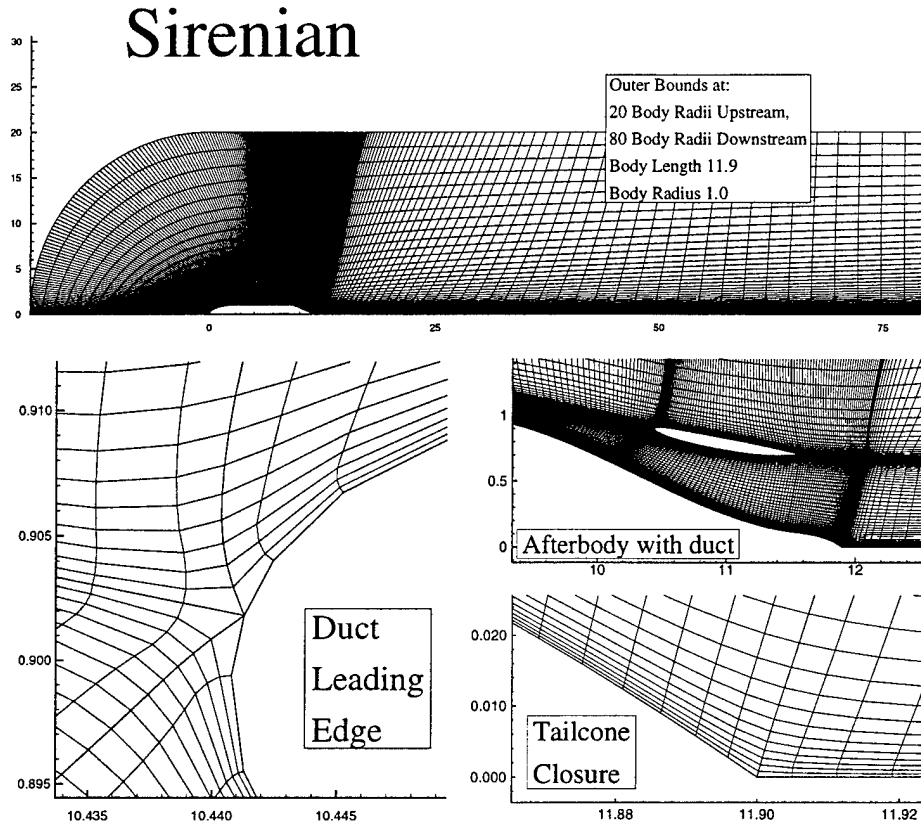
Figure 3-2: The RANS grid used to model the Sirenian body.

3.2.3   Rotor / Stator design

The coupled lifting surface / RANS design method requires iteration on many levels. Figure 3-3 shows the many iterations paths to reach a fully converged and balanced solution.

The final product of the Sirenian design is shown in Figure 3-4. The stator and rotor blade can be seen through the cut-away view of the duct. The Sirenian design models a body of revolution; no appendage drag is considered.

When performing preliminary design, several items are of recurring importance. They are:

- **Swirl.** The most efficient propulsor will not necessarily have full tangential velocity cancellation in the wake. The additional momentum needed to fully
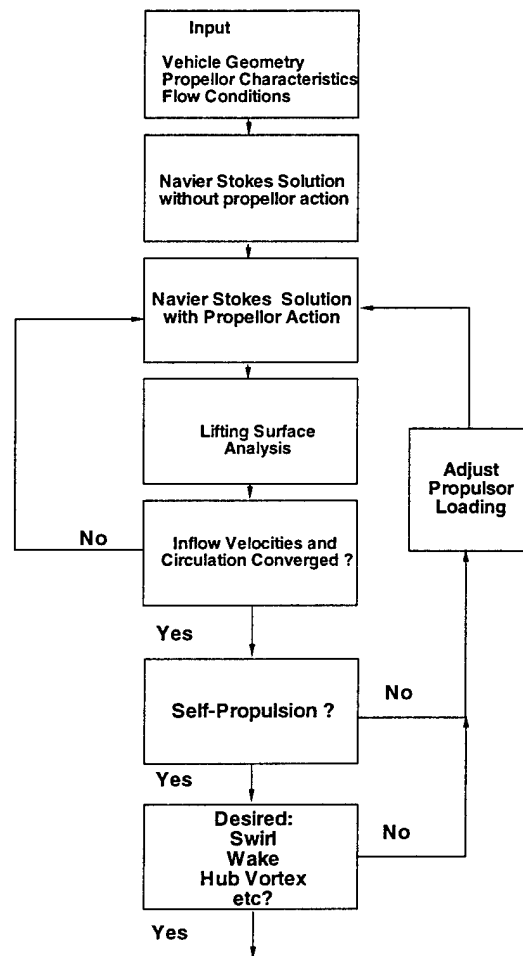
Figure 3-3: General procedure for the Navier Stokes / Propeller Blade Design of a vehicle with a propulsor.
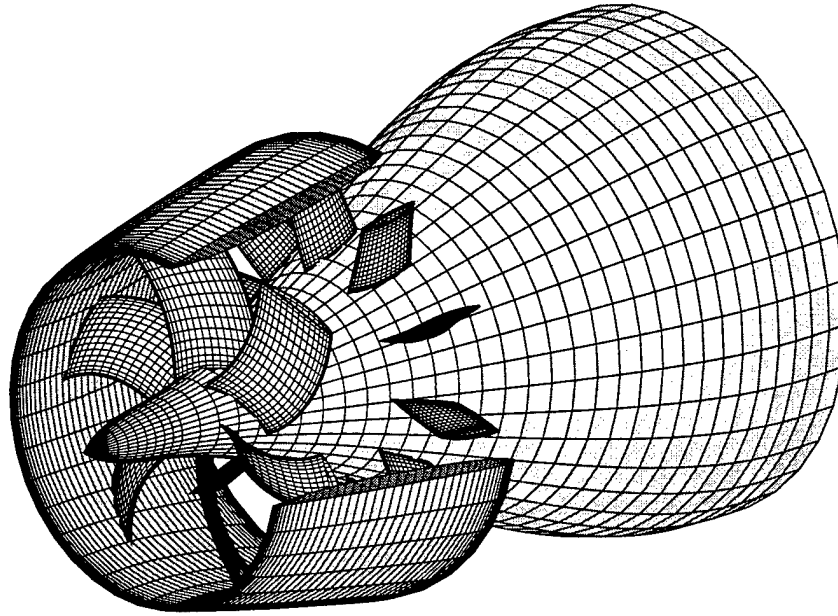
Figure 3-4: Afterbody of the Sirenian propulsor design.

cancel the tangential velocity will have an associated viscous drag penalty on the blades. Conversely, the presence of a hub vortex is undesirable so swirl cancellation near the hub is generally desired.

- **Boundary Layer Ingestion.** An efficient design will ingest the entire boundary layer into the propulsor. There in, the kinetic energy used to build the boundary layer is potentially recovered.

- **Wake Profile Aft of the Body.** The axial velocity profile left in the wake of the body should be as uniform as possible. Ideally, the body would leave a wake that is uniform and equal to the inflow velocity. Thus, it would pass through the fluid and then leave the fluid "undisturbed."

- **Drag and Thrust Balance.** At the design advance coefficient (J_s), the drag

of the body and appendages must be exactly overcome by the thrust of the propulsor. To achieve this balance, the blade loading on the stator and rotor must be adjusted while also maintaining the desired amount of swirl cancellation.

- **Duct Loading Fraction.** The duct loading can be varied during the design stage to evaluate the overall effect on the propulsor efficiency. Performance of accelerating and decelerating nozzle arrangements are discussed in many references such as [21]. Additionally, shifting thrust to the duct allows the blades to be less loaded and improve the cavitation characteristics of the propeller.

Lifting Surface / RANS

To ensure a converged solution is reached, the mass flow through the propulsor and the coefficient of thrust and torque (K_T, K_Q) are tracked during the coupled lifting surface / RANS procedure. A sample convergence history for a (2%) change in advance coefficient is shown in Figure 3-5.
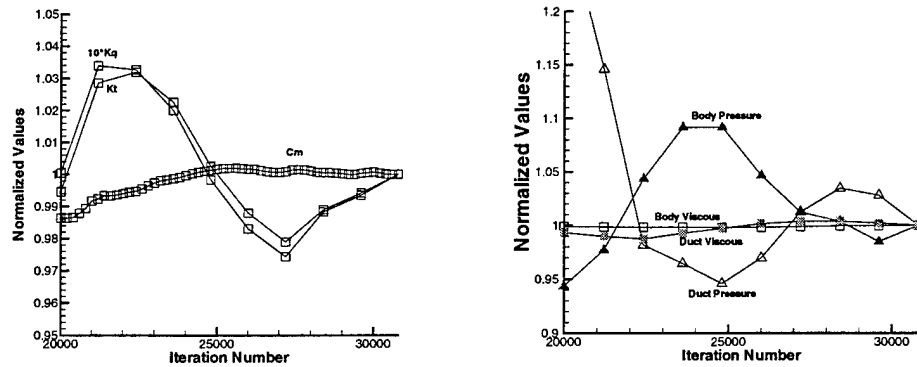
Figure 3-5: History of thrust, torque and mass flow rate, and of body and duct drag following a 2% perturbation in advance coefficient.

As would be expected, the viscous drag on the body and on the duct does not vary significantly with the small change in the advance coefficient. Conversely, the pressure drag makes significant swings, as much as 30 percent.

For this design, the boundary layer is fully ingested into the duct as shown in

29

Figure 3-6. Additionally, the tangential velocity is shown as a contour plot. The inflow velocity is 1.0. The large swath of tangential velocity in the wake is a hub vortex caused by non-cancelling circulations. Aft of the body centerline, there is a strong hub vortex and an axial velocity less than free stream. These indicate that this design could be improved through more iterations of the blade circulation.

The streamline forward and aft of the duct shows how much of the boundary layer is ingested in the propulsor. As discussed by Thurston and Evanbar, the most efficient design would have the entire boundary layer ingested to recover the kinetic energy in the boundary layer [29]. The wake profile should then be as uniform as possible at a constant velocity equal to the inflow velocity.
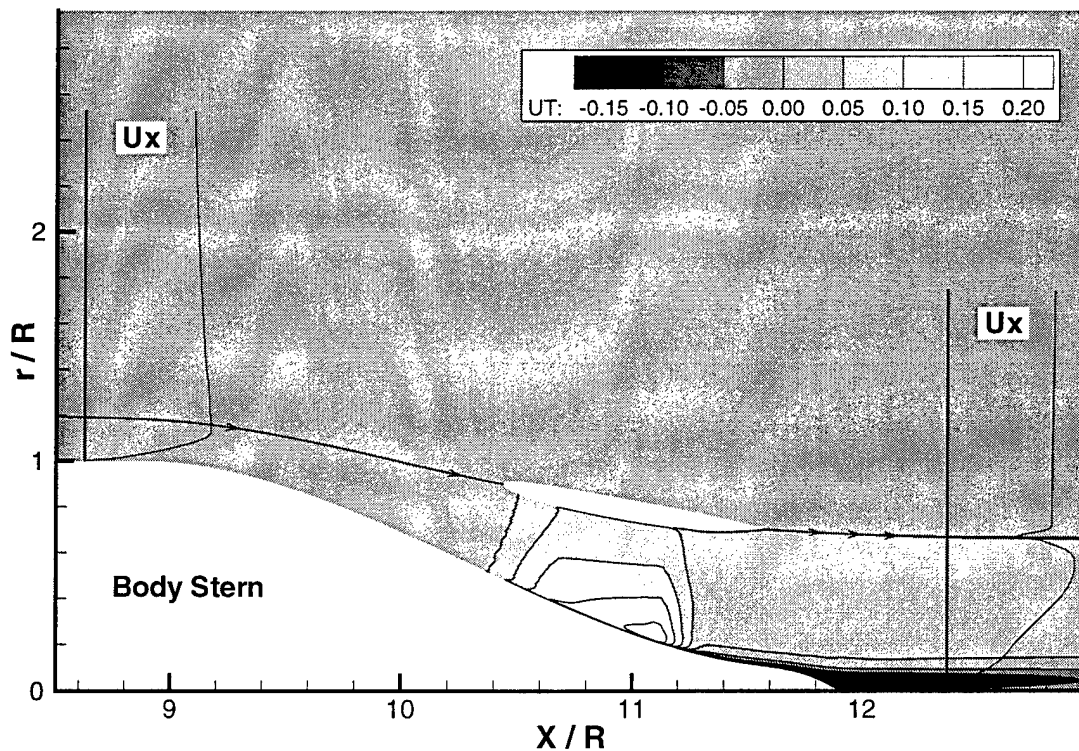
Figure 3-6: Boundary layer profiles and the duct streamline are shown for a full stern design.

In reviewing Figure 3-6, the aftmost boundary layer profile indicates that some

improvement in the efficiency of the propulsor is possible. The boundary layer has a hump greater than the inflow velocity at about r/R equal to 0.5, this hump causes proportionally more kinetic energy to be left in the wake. Kinetic energy is proportional to $V*V$, whereas thrust is proportional to V, thus exceeding the inflow velocity tends to waste more energy. Similarly, in Figure 3-6, there is a depression in the wake profile near r/R of zero. The depression indicates that by directing more flow aft, and incidentally less in swirl, the efficiency could also be improved.

Improvements to the design are easily identified. However, actually accomplishing these improvements is tedious and time-consuming. The improvements are largely based on engineering judgment and checked with detailed numerical solutions.

3.3 Model Scale Powering Characteristics

Recall this propulsor / body combination does not represent an arrangeable submarine as developed in Chapter 2. Rather, this combination is just a representative estimate of a submarine. It does not include appendage drag and the frictional drag has not been adjusted to a full scale value. The powering results are shown in Table 3.1.

	Sirenian
$C_{D_{SHIP}}$	0.1253
$C_{T_{SHIP}}$	0.1313
$PercentOverpowered$	4.5
K_T	.2301
$10 * K_Q$	.4801
$PowerCoefficient$	0.113

Table 3.1: Results for the Sirenian model scale design.

Chapter 4

Full Scale Design of Sirenian

4.1 RANS Grid

The RANS grid has been shortened compared to the original Sirenian grid. The main reason for this is two fold. First, since comparing propulsor geometries affects the afterbody only and having an identical bow does not change the inflow properties, the grid size can be reduced to save computational time. Secondly, variations originating at the bow due to numerical instabilities could lead to errors in the comparisons. The pressure drag tends to behave erratically and does not consistently settle to stable value. Figure 4-1 shows the variations of pressure on the body and the duct over 1000 RANS iteration cycles. The afterbody evaluation of pressure seems consistent. However, the evaluation of pressure near the bow and, thus, the evaluated pressure drag is unusable. These errors originate from numerical instabilities induced from the RANS grid spacing across the zonal junction near the bow.

First, to solve this difficulty, the body pressure drag is evaluated using a geometrically generated RANS grid on a similar body. Secondly, to provide an independent check, the body pressure drag is evaluated using an Integral Boundary Layer method. The results are encouraging. Figure 4-1 shows the comparison. For full scale Sirenian and for later variants, the RANS solution solves the afterbody portion of the flow only and uses the stable, geometrical gridded, solution as a boundary condition at
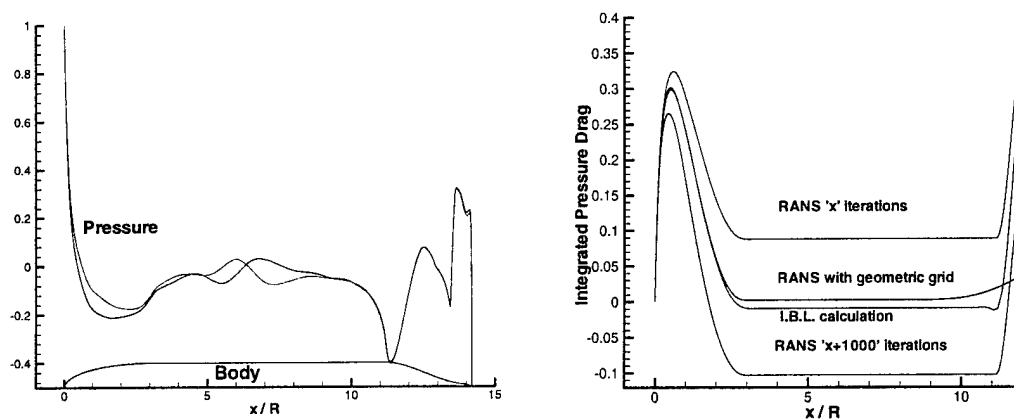
Figure 4-1: The figure on the left shows the body pressure variations over 1000 RANS cycles in a stabilized flow field. The figure on the right shows the resultant body pressure drag integrated over the body for identical inflow and bow/midbody geometry. Variations between the methods are expected near the propulsor due to different assumed propulsors and stern fullness.

the upstream edge of the grid.

Another difficulty presents itself when establishing a RANS grid for the first time. The boundary layer tends to develop a discontinuity across the grid junction if the grid spacing and grid orthogonality are not matched closely across the grid junction. The difficulty can be minimized by matching the grid vertical spacing across the junction along the entire boundary axial extent.

The boundary layer discontinuity can be made a null issue by ensuring the grid boundary follows a streamline. This ensures that no fluid needs to cross the boundary. The streamline is not known *a priori*. Consequently, using an open water case streamline then replacing it with the new ducted case streamline provides a mechanism to alleviate the boundary layer discontinuity. It should be noted that the streamline location changes when the thrust is changed. Thus, to a small extent, the grid zonal boundary is iterative with the thrust.

33

4.2 Full Scale Estimates

In Chapter 3, Sirenian matches drag and thrust on the model scale after solving the vortex lattice / RANS coupling. To allow Sirenian to be more representative of a real submarine, the effects of model verses full scale are considered. Using the ITTC friction line estimate, the model scale and full scale frictional drag are calculated and, after correctly non-dimensionalizing the quantities, are used to scale the Sirenian to full scale. Equation 4.1 shows the relationship.

$$C_{D_{Ship}} = C_{D_{Model}} - C_{Df}(\Re_{Model}) + C_{Df}(\Re_{Ship}) + C_{D_{allowance}} + C_{D_{appendage}} \qquad (4.1)$$

The model drag is summed in the calculations as in equation 4.2.

$$C_{D_{Model}} = C_{D_{BP,x<8}} + C_{D_{BP,x>8}} + C_{D_{BV,x<8}} + C_{D_{BV,x>8}} + C_{D_{DP}} + C_{D_{DV}} + C_{D_{Stator}} \qquad (4.2)$$

For different designs, the frictional drag at full scale will vary. However, the changes in the actual frictional coefficient are neglibly small. To illustrate by example, the assumed full scale condition for all Sirenian frictional coefficients is 199 feet and 22 knots. A change of 1 knot in speed results in a 0.6 % difference in $C_{Df}(\Re_{Ship})$. Similarly, 5 knots results in 2.6 % difference. Recall, the Sirenian is not scaled to correspond to the variants of the arrangement study; these will be examined in the following chapters.

A correlation allowance of 0.0005 (non-dimensionalized on wetted surface area) is used for all variants. The appendage drag is calculated using Hoener's relationship as discussed in [23]. The appendage drag is expected to add a fixed amount to the C_D of 0.022. This additional drag represents about 15% to 20% additional appendage drag and is consistent with other references such as Burcher and Rydill [4]. Table 4.1 summarizes the corrections used to extrapolate the model scale drag to full scale.

Coefficient	Value
$C_{Df}(\mathfrak{R}_{Model})$	-0.08778
$C_{Df}(\mathfrak{R}_{Ship})$	0.04032
$C_{Dallowance}$	0.01229
$C_{Dappendage}$	0.0220
Total Correction	-0.01316

Table 4.1: Corrections used to extrapolate the model scale Sirenian drag to full scale drag.

4.3 Powering Characteristics of a Full Scale Sirenian

The ultimate goal of a design such as this one is to maximize the speed with the install power. Assuming no hub, and therefore nearly constant diameter helices in the wake, the optimal circulation distribution on a blade set in a duct is constant distribution. The upstream blade set induces a circulation which is exactly canceled by the downstream blade set. Reference [20] discusses this further.

For the full stern, the helical wake contracts significantly and has a pronounced strong interaction with the rest of the propulsor elements. A constant circulation is used as a starting point for this design. Variations from constant are used to explore other designs.

4.3.1 Circulation Distribution

For all Sirenian designs, the circulation distribution is linear. The slope of the distributions vary to provide a range of cases to evaluate. The constant case uses the non-dimensional circulation of 0.0110 on the rotor and $0.0110 * (6/11)$ on the stator. This ratio of rotor loading to stator loading provides nearly complete swirl cancellation.

The tip loading in excess of the $r/R = 0.7$ value (0.0110) is used to gage the various cases. When varying the circulation, the stator value is adjusted by the same tip loading excess times the factor 6/11 to account for the different number of blades. Finally, the magnitude of blade loading is adjusted to make the overall thrust and drag equal within a few percent. Adjusting the magnitude made the percent of actual

excess loading change when the distribution is uniformly scaled to achieve a balanced thrust and drag. Figure 4-2 illustrates these ideas.
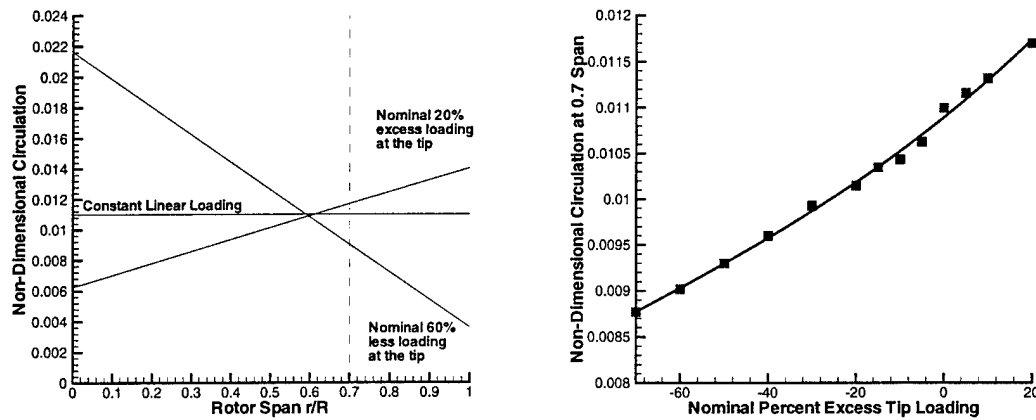
Figure 4-2: The left most figure shows representative non-dimensional circulation distributions. The figure on the right denotes how the actual value of non-dimensional circulation at the 0.7 span changes to maintain a balanced thrust and drag condition.

4.3.2   Results of Circulation Distribution Variations

Table 4.2 summarizes the evaluated cases. The thrust and drag are balanced within ± 1.0% for all cases. Note, however, the thrust and the drag both increase as the hub is loaded more. Since higher hub loading causes higher velocities close to the body, the frictional drag is increased. This is analogous to a higher thrust deduction. Additionally, the higher hub loading tends to produce a hub vortex which adds to the body drag. The combination of more frictional drag and more hub vortex drag is offset by the higher hub loading. Increasing the hub loading, provides more thrust with less penalty in the require torque since the radius from the hub is smaller. Thus, more hub load provides an overall benefit to the ship's powering characteristics.

4.3.3   Conclusion on Blade Loading

The minimum power for a given case is directly related to the torque coefficient, K_Q. Since $P = 2\pi n Q$ and using the definitions of K_T, K_Q and J_s, the case with the best

	$C_{D_{SHIP}}$	$C_{T_{SHIP}}$	$Overpowered$	K_T	$10 * K_Q$	$PowerCoef.$
20%G	0.08916	0.08836	-0.9	0.2209	0.4426	0.0732
10%G	0.08907	0.08972	0.7	0.2243	0.4417	0.0730
5%G	0.09048	0.09080	0.4	0.2270	0.4422	0.0731
$Constant$	0.09136	0.09188	0.6	0.229	0.4430	0.0733
5%L	0.09162	0.09092	-0.8	0.2273	0.4336	0.0717
10%L	0.09245	0.09160	-0.9	0.2290	0.4323	0.0715
15%L	0.09326	0.09324	0.0	0.2331	0.4352	0.0720
20%L	0.09357	0.09368	0.1	0.2342	0.4320	0.0714
30%L	0.09596	0.09632	0.4	0.2408	0.4347	0.0719
40%L	0.09742	0.09760	0.2	0.2440	0.4323	0.0715
50%L	0.09899	0.09900	0.0	0.2475	0.4311	0.0713
60%L	0.10043	0.10032	-0.1	0.2508	0.4294	0.0710
70%L	0.10203	0.10188	-0.1	0.2547	0.4297	0.0711

Table 4.2: The results associated with the non-dimensional Sirenian body / propulsor combination indicate higher hub loading provides better powering characteristics.

speed is the same case that has a minimum value of K_Q. The trend clearly shows that less tip loading gives a better design when considering speed for a given installed horsepower. Some variations in the trend are related to small deviations in the vortex lattice / RANS coupling process. Yet, the overall trend is evident and is graphically shown in Figure 4-3.

The trends seems to continue past the values evaluated. The difficulty becomes the excessive lift coefficient required to generate the specified hub loading. Using a typical lift coefficient upper limit of 0.4 to 0.5, the 60% less tip loading case seems to reach the reasonable design limit. Figure 4-4 shows the lift coefficient verses span for the 60% less tip loading case.

Reviewing the axi-symmetric flow field from the RANS output gives the reason for the trend toward higher "efficiency" with higher hub loading. The velocity in the wake of the body tends to get filled in by higher velocity fluid. The wake deficient velocities are brought closer to the free steam velocity. As the wake is filled in, the wake profile approaches a uniform, constant velocity. In light of the discussion in Section 3.2.3, the trend that higher hub loading gives higher efficiency is reasonable.

The trend can also be evaluated using the wake deficient analogy. The body produces a thick boundary layer upstream of the propulsor. As this boundary layer
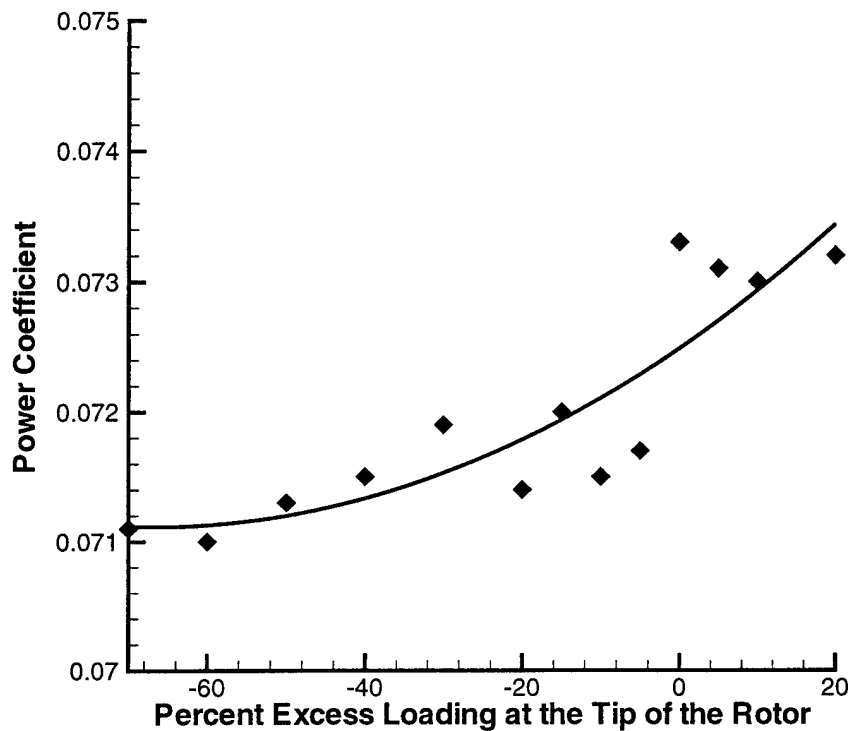
Figure 4-3: The variation of C_P shows higher hub loading minimizes the power.

approaches the propulsor, the fluid closest to the body has the most kinetic energy. Thus, to recover this energy, the fluid closest to the body needs accelerating the most. Hence, higher loading at the hub is needed to recover the energy in the boundary layer.

Finally, by loading more heavily at the hub, the tip loading is reduced. This has the benefit of reducing likelihood of tip cavitation. While this conclusion finds that 60% nominal less loading at the tip is a good design, it is not "optimal." More studies are needed to confirm that this trend holds given other constraints. Additionally, variations from the linear distribution may yield even better results.

4.3.4 Propulsive Coefficient

Now that the propulsor characteristics are calculated, can a propulsive coefficient (PC) be calculated? In short to calculate a PC, the unpropelled drag on the towed
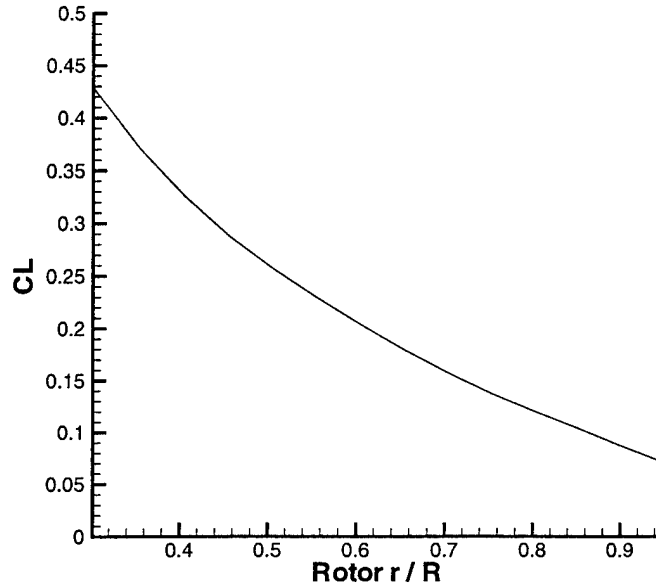
Figure 4-4: For the 60% less tip loading case, the coefficient of lift on the blade approaches 0.5. Separation will likely occur at C_L higher than about 0.4 to 0.5.

body must first be estimated. The difficulty here lies in the fact that the unpropelled body will exhibit separation near the stern, and present day numerical methods cannot accurately model the separated flow dynamics.

The propulsive coefficient measures the effective horsepower out of the system divided by the shaft horsepower put into the system. The effective horsepower is towed resistance times the velocity of the ship. The towed resistance, R_T, is related to the propeller thrust by a thrust deduction factor [21].

$$PC = \frac{EHP}{SHP} \qquad (4.3)$$

$$EHP = R_T V_s \qquad (4.4)$$

$$R_T = (1 - t)T \qquad (4.5)$$

The towed resistance (i.e. unpropelled resistance) for a full stern is quite large due to separation on the after part of the ship when compared to its propelled resistance. Separation is prevented by the action of the propulsor. Generally, when the separation is removed by the action of the propulsor, the hull drag will decrease. The effect of a large unpropelled resistance will make the EHP larger for a given speed. Accordingly, a full stern PC will be higher than a conventionally tapered stern PC. While the PC will be higher, this does not lead to the conclusion that the maximum speed will be higher.

The maximum PC attainable can be larger than 1.0 [29], [21], [27]. Neglecting shaft losses ($\eta_S = 1.0$), the PC for the 60% less tip load case is $1.41(1 - t)$. Using equation 4.5, we know that $(1 - t) > 1$. Thus, the PC will be some value greater than 1.41. This does not lead to the conclusion that this design will have a higher speed than a design with a lower PC. The conclusion is that the propulsor in this design does a better job of propelling the body verses the body being towed.

Using a PC for a full stern design is very misleading. The speed, thrust, and torque can be calculated directly from the coefficients obtained in a coupled lifting surface / RANS analysis. The best measure of full stern performance is the maximum speed attainable for a given installed horsepower. Understandably, however, an "efficiency" is desired to use during comparisons. One "efficiency" that measures power is the Power Coefficient, C_P. The Power Coefficient is defined in equation 4.6 and is shown in Table 3.1 and Figure 4-4 for this design.

$$C_P = \frac{2\pi n Q}{\frac{1}{2}\rho V_S^3 A_B^2} \tag{4.6}$$

Each of the variables are defined in the nomenclature section. The C_P represents the power input to the propeller divided by a power associated with the ship speed and the frontal area of the body.

Chapter 5

Lifting Surface / RANS Evaluation of Variant 3

The Sirenian propulsor attributes are combined with the results from the arrangement study to form a physically realizable submarine variant. In order to estimate the maximum speed attainable from the installed 5500 SHP, the variant is evaluated for K_T and K_Q. The trends of Chapter 4 are applied to this full stern variant. A sampling of cases are used to evaluate the maximum hub loading without separation. Then, the blade loading is adjusted to refine the boundary layer in order to maximize speed. Finally, various body stern geometries are used to reduce the drag in order to increase speed.

5.1 Physical Geometry

The Variant 3 has a total body length of 14.2 and a body radius of 1.0. The bow is identical to the bow used for Sirenian. This similarity aids in direct comparisons of propulsor changes. The bow is elliptical to $x/L = 3.0$, parallel midbody from 3.0 to 11.2, then the same two cubic polynomials used in the Sirenian design close the body. Other afterbody shapes are discussed in section 5.4. The design Reynolds number for the RANS computations is 268829 based on body radius. The duct chord is 1.15 with t/c of 0.08 and f/c of -0.02 at a 10 degree angle of attack. The duct has been moved inward to capture less of the free stream and place the leading edge at the

	$C_{D_{SHIP}}$	$C_{T_{SHIP}}$	$Overpowered$	K_T	$10*K_Q$	$PowerCoef.$
20%G	0.12259	0.12192	-0.5	0.3048	0.6271	0.1037
$Constant$	0.12620	0.12568	-0.4	0.3142	0.6160	0.1019
20%L	0.13140	0.13076	-0.5	0.3269	0.6112	0.1011
40%L	0.13704	0.13676	-0.2	0.3419	0.6140	0.1015
60%L	0.14288	0.14385	0.7	0.3596	0.6228	0.1030

Table 5.1: The results associated with the non-dimensional Variant 3 indicate that the nominal 20% less tip loading case has the best powering characteristics.

	$Thrust(lbf)$	$ShaftRPM$	$Torque$	$MaxSpeed(knt)$
20%G	98142.	84.81	340601.	21.47
$Constant$	102380.	85.32	338580.	21.60
20%L	107076.	85.54	337698.	21.65
40%L	111648.	85.41	338213.	21.62
60%L	116319.	85.01	339821.	21.52

Table 5.2: The results assume a submarine length of 199 feet and 5500 SHP.

"knee" of the boundary layer.

The stator has 11 blades with the leading edge tip at $x/L = 12.7948$ and $r/R = 0.740817$. The rotor has six blades with its leading edge tip at $x/L = 13.3854$ and $r/R = 0.602437$. There is no gap between the blades and the duct. The design J_s is 1.52. The selected RANS grid is similar to the RANS grid used to calculate the Full Scale Sirenian. The grid starts at x=8.0 and extends to x=80.

5.2   Results of Circulation Distribution Variations

Table 5.2 assumes a physical submarine that matches Variant 3 from the Chapter 2 arrangements study. Since the length to diameter ratio of Variant 3 is already selected to match the Chapter 2 study, the only additional assumptions are a length of 199 ft and an installed power plant of 5500 SHP. Using a linear blade loading distribution, a gain of 0.2 knots on the maximum speed is possible when the tip has 20% less nominal tip loading. The design process undertaken uses the propeller torque and RPM as variables, not fixed at the onset. This is consistent with the use of electric drive with solid state speed controllers as used in the arrangements study of Chapter 2.

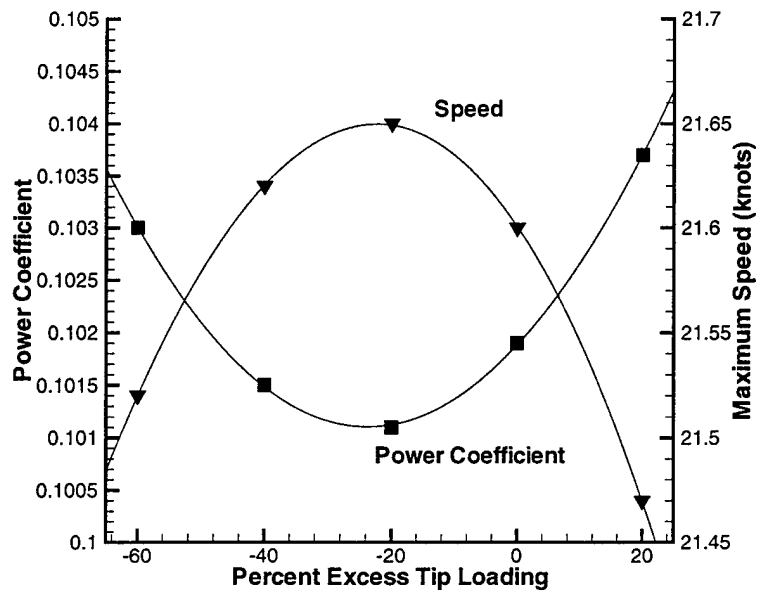Figure 5-1: The trend shows that a higher hub loading minimizes the power until the loading is so high that other influences such as frictional drag, hub vortex, etc. offset the gains.
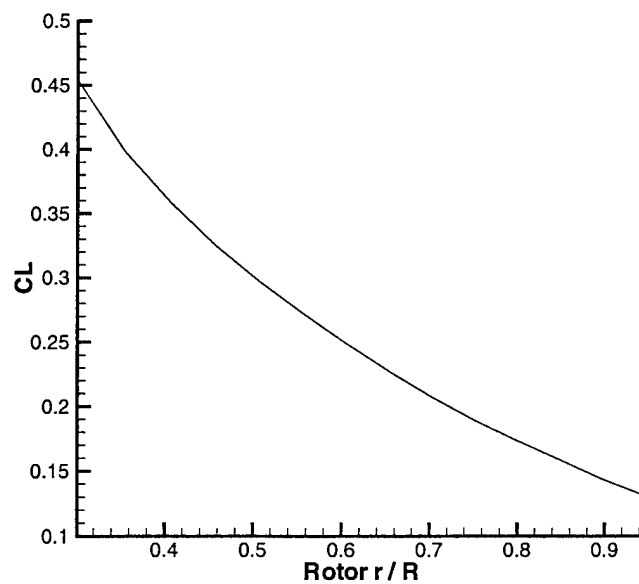
Figure 5-2: For the 20% less tip loading case, the coefficient of lift on the blade approaches the highest that can be reasonable obtained. As the C_L approaches 0.5, separation will likely occur at the rotor hub.

The local optimal of the 20% less tip loading case has the lowest power coefficient and thus the highest speed as shown in Figure 5-1. Additionally, this case has the highest rotor lift coefficient that can be reasonably obtained. Figure 5-2 shows the lift coefficient for this case.

5.3 Blade Loading at Hub

Thus far, more hub loading gives better powering characteristics. However, when the blade loading causes the blade section coefficient of lift to exceed a reasonable value, the cavitation and flow separation on the blade is likely. To capitalize on these trends, the blade loading is adjusted from a linear distribution to a distribution which loads the blade hub more without exceeding a lift coefficient of about 0.45.

The revised blade loading uses the 20% less tip loading case and then, on the blade sections less than about 30% span, the blade loading is reduced. Finally, the blade loading is adjusted so that a reasonable coefficient of lift is reached on the lower 30% of the blade. The blade loading and the resulting lift coefficient are shown in Figure 5-3. Table 5.3 gives the powering characteristics.

5.4 Body Stern Geometries

Figure 5-4 shows the integrated drag due to pressure and viscous influences on the two-cubic polynomial Sirenian afterbody. Considerable drag occurs on the body near the propulsor entrance way. The body and the duct have a strong interaction on each other's drag components. The interaction of the duct on the body plays a role in the total drag on the body. In this case, the body drag is considerable while the duct actually provides a net thrust.

The effects of body profiles are studied to better understand the sharp rise in drag near the propulsor. The boundary layer is highly sheered as it is accelerated towards and through the propulsor. Due to the sheered flow near the propulsor, an increase

44
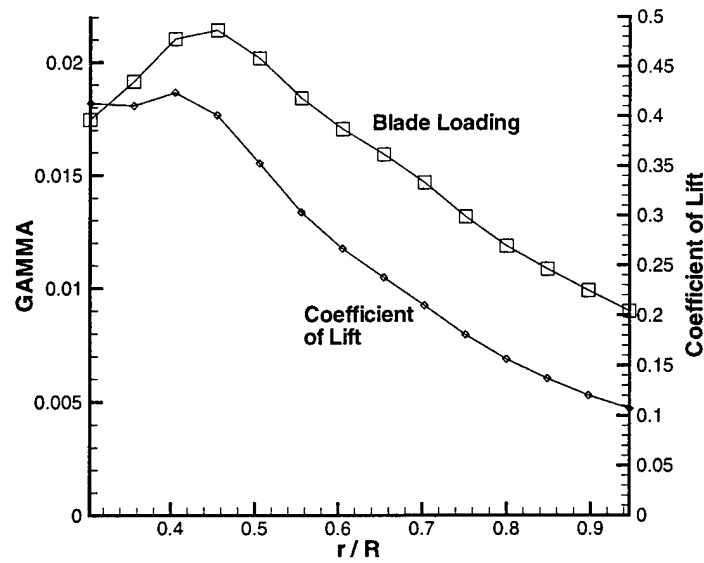
Figure 5-3: The best results load the hub so that the lower one-third of the blade has a lift coefficient that approaches the maximum attainable without blade flow separation. Other blade loading distributions which build on these trends could provide even better results.

in the viscous drag is expected. A corresponding increase in the pressure drag is also expected, although the anticipated magnitude and shape are less clear.

To mitigate the increase in drag near the propulsor, a smoother transition is needed as the flow is redirected from the parallel midbody into the propulsor. The chosen functions, $y = x/(1 + x)$ and $y = tanh(x)$, are used to provide a general shape. To cast the functions into the shape of a full stern, the functions are multiplied by constants so that their shape matches the original Sirenian shape at the stern. Finally the functions are joined with a third-order polynomial to close the stern. For all geometries, the transitions maintain a continuous first and second derivative to alleviate pressure discontinuities in the flow. Figure 5-5 shows the three body profiles and their derivatives.

From the cases studied, the geometry which has the smoothest transition, i.e. continuous higher order derivatives, is also the geometry which has the best powering characteristics. The fractional case, $y = x/(1 + x)$, has 21% less drag than

45
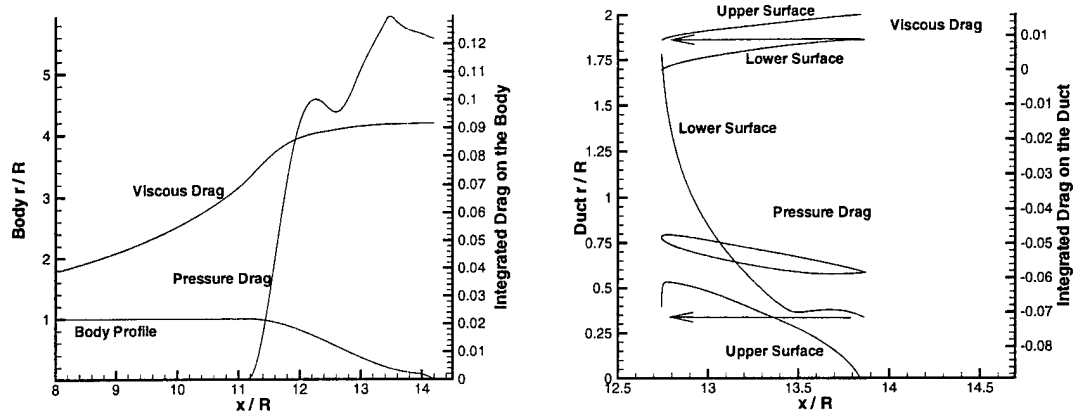
Figure 5-4: The integrated drag due to pressure and viscous influences are shown for the Sirenian afterbody. One method to improve the powering characteristics is to reduce the sharp rise in the drag at the entrance of the propulsor.

Shape Function: Blade loading:	cubic poly. linear	cubic poly. modified	$y = x/(1+x)$ modified	$y = tanh(x)$ modified
$C_{D_{SHIP}}$	0.1314	0.1300	0.1029	0.1017
$C_{T_{SHIP}}$	0.1308	0.1297	0.1029	0.1018
$PercentOverpowered$	-0.5	-0.3	0.1	0.1
K_T	0.3269	0.3242	0.2573	0.2544
$10 * K_Q$	0.6112	0.6058	0.4884	0.4771
$PowerCoefficient$	0.1011	0.1002	0.0808	0.0789
$Thrust(lbf)$	107076.	106821.	97871.	98290.
$ShaftRPM$	85.54	85.79	92.18	92.90
$Torque(ft-lbf)$	337698.	336700.	313371.	310936.
$MaxSpeed(knots)$	21.65	21.72	23.34	23.52

Table 5.3: The smoother the body profiles, the better the powering characteristics.

the cubic polynomial geometry of the Sirenian afterbody. The hyperbolic tangent case, $y = tanh(x)$, has 22% less drag than the Sirenian afterbody. The later case has the smoothest transition from the parallel midbody to the propulsor. Table 5.3 summarizes the powering characteristics.

5.5 New Body Geometries

The general trends need to be identified to establish the characteristics of a optimum powering full stern body. The techniques used throughout this thesis can be used to establish the trends. By studying the flow details around a series of bodies, the trends

46
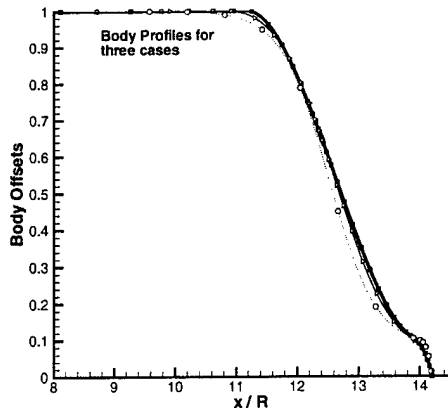
(a) The body profiles are shown with an exaggerated ordinate scale. The bold line and open square symbols show the original body profile. The fractional body is shown with right triangles. The hyperbolic tangent body is shown with a dotted line and circles. Note the close similarity in the body profiles.
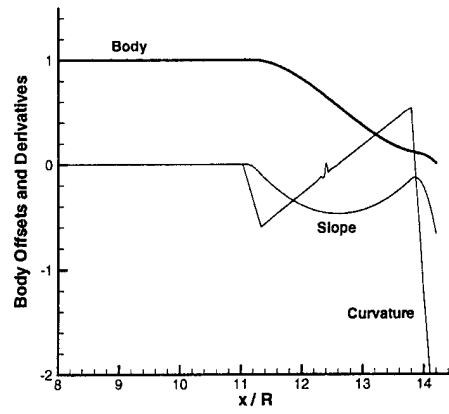
(b) The Sirenian body profile and the corresponding first and second derivatives are shown above. The Sirenian uses two third-order polynomials to represent the body in the propulsor region.
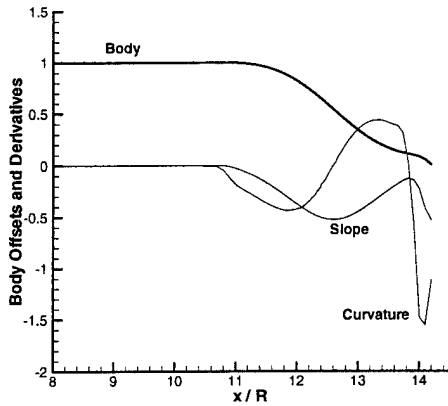
(c) This version uses the curve $y = x/(1 + x)$ to provide the curvature near the propulsor. A third-order polynomial is used from 13.9 to 14.2 to close the body. The first and second derivatives are smoother than the original Sirenian body.
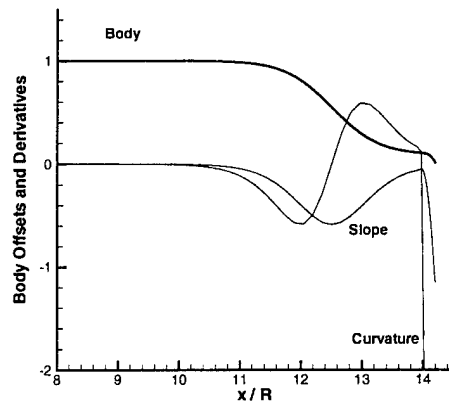
(d) This version uses a $y = tanh(x)$ curve to provide the curvature near the propulsor. A third-order polynomial is used from 13.9 to 14.2 to close the body. The first and second derivatives are smoother than the other bodies. This version has an infinite number of continuous derivatives in the region on $x/L = 11$, which is where a great reduction is achieved in both body pressure and viscous drag.

Figure 5-5: Body profiles and derivatives

47

can be developed and applied to a parent body to establish an optimum design.

Future studies can use the results contained herein to establish a parent hull form. The new parent hull form could serve as a central point for the variations of each characteristic. As long as the tested characteristics are close to the parent hull form characteristic, the results should extend to the case where several characteristics are simultaneously changed to their respective optimal value. While this idea does not optimize the whole body at once, it does give a reasonable approach to an extremely broad problem.

In order to ensure continuity in higher derivatives to minimize drag, the parent hull form should be constructed out of a single mathematical function. One possibility is the use of B-splines. B-splines describe the body with much fewer control points. The order of the B-spline curve is determined by the number of constraints placed on the B-spline.

A second possibility is the use of a power series of the form, $y^2 = a_1 x + a_2 x^2 + \ldots + a_n x^n$, where x is the non-dimensional abscissa and y is the non-dimensional ordinate. The arbitrary constants a_1, a_2, etc. for each form are determined by the geometrical properties of the form. The number of constants is determined by the number of constraints on the body.

The constraints include the body properties such as $y(L) = 0$ and the naval architecture characteristics such as the aft prismatic coefficient C_{Pa}. The following list shows possible constraints for a full stern body series.

- Assuming the power series describes only the curved afterbody, continuity of derivatives should be maintained by specifying position and derivatives at the parallel midbody and afterbody junction. As a minimum, the slope and curvature should be matched. However, matching higher derivatives is expected to improve powering. An alternative method describes both the parallel midbody and the afterbody with the power series. This method still requires specify-

48

ing derivatives to ensure the parallel midbody is maintained up to a specified location.

- The radius of curvature can be specified at the three primary locations on a full stern body. Moving aft along a typical full stern afterbody, the curvature will first have a large negative maximum at the shoulder, a large positive maximum somewhere in the middle and, finally, a large negative maximum as the body closes. Both the (x, y) location and the magnitude of maximum curvature can be specified for each location. The radius of curvature is given by:

$$\rho(x) = \frac{[1+(\frac{dy(x)}{dx})^2]^{3/2}}{\frac{d^2y(x)}{dx^2}}$$

The location could be specified by $y(x_1) = y_1$ where x_1 is determined from $\frac{d\rho(x_1)}{dx} = 0$.

- The prismatic coefficient can be specified in the power series representation. The constraint is of the form: $C_{pa} = \frac{1}{R_B^2 L_a} \int_{L_a} y(x)^2 dx$ where L_a is the length of the afterbody.

- The length to diameter ratio can also be specified by the location of the tail cone.

- The duct characteristics must be somehow integrated in the body series study. The duct characteristics which could be varied include: angle of attack, thickness and thickness distribution, camber and camber distribution, location of duct with respect to the body, location of the duct with respect to the rotor and the radius of the duct inner surface.

- Since the full stern body must be evaluated while under power to capture the dynamics of the boundary layer, characteristics of the propulsor blades must also be included in a body series. These characteristics include: blade loading distribution and division of loading between the stator and rotor.

49

Chapter 6

Lifting Surface / RANS Evaluation of Variant 4

The next comparison evaluates the arrangements variant 4. This case represents a more typical submarine afterbody shape than the full stern Variant 3. The typical case uses the same elliptical bow as all other variants and uses the Huang 1 afterbody [17]. The overall length is achieved by varying the amount of parallel midbody to match the Variant 4 length to diameter requirement. Both a non-ducted and a ducted version are evaluated.

6.1 Non-Ducted Tapered Body Evaluation

6.1.1 Physical Geometry

The Huang 1 afterbody is used to represent typical tapered stern submarine geometry, as well as typical propeller placement and characteristics. Since this case represents a typical case, the given geometry and placement are taken as optimum given realistic constraints on the design.

Figure 6-1 shows a notional sketch of the geometry. Consistent with reference [17], the design has seven blades with the leading edge tip at $x/L = 17.1$ and a r/R at the tip of 0.545. No duct nor pre-swirl vanes are present. The design J_s is 1.25.

Using similar methods to those used in section 4.2, the full scale corrections were developed and are shown in Table 6.1.
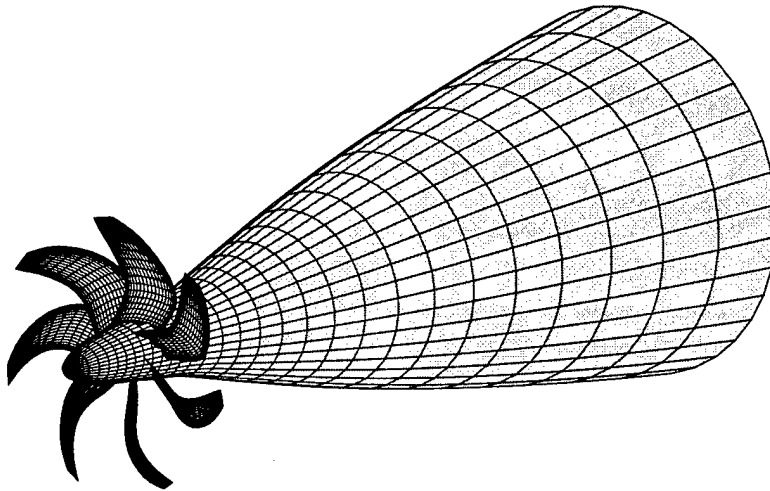
Figure 6-1: Notional tapered stern non-ducted design

Coefficient	Value
$C_{Df}(\Re_{Model})$	-0.09944
$C_{Df}(\Re_{SHIP})$	0.04481
$C_{D_{allowance}}$	0.01446
$C_{D_{appendage}}$	0.0220
Total Correction	-0.01817

Table 6.1: Corrections used to extrapolate the tapered stern results to full scale drag

	Tapered with No Duct
$C_{D_{SHIP}}$	0.09624
$C_{T_{SHIP}}$	0.09570
$PercentOverpowered$	-0.7
K_T	.1977
$10 * K_Q$	.3806
$PowerCoefficient$	0.0926
$Thrust(lbf)$	83064
$ShaftRPM$	118.4
$Torque(ft - lbf)$	244023
$MaxSpeed(knots)$	22.3

Table 6.2: Results for the open water propeller

6.1.2 Powering Characteristics

The circulation distribution used for the open water case is assumed to be an optimum distribution based on previous work [17], [20]. The powering results are shown in Table 6.2. By using the same technologies for this variant as the full stern variant, neither the torque nor the shaft speed have limits imposed. Consequently, they are free to float to the values that best optimized the propulsor design.

6.2 Ducted Tapered Body Evaluation

6.2.1 Physical Geometry

The Variant 4 ducted design uses as much in common with the non-ducted Variant 4 and with the full stern Variant 3, as possible. As such, the duct chord is 1.15 with t/c of 0.08. However, due to massive separation on the duct outward side when the camber and angle of attack matched the original values, the f/c is 0.01 with a 6 degree angle of attack. To reduce the separation on the duct, the inner surface of the duct is aligned with the streamline in the open-water propelled case that passed through the location of the propeller tip. The rotor tip is placed at the same axial location on the body as in the non-ducted case. The reduced camber and reduced angle of attack will cause the duct to generate less lift in the direction of forward thrust.

The radial placement of the duct inner surface is place using the ideas presented in reference [15]. The placement maintains the same thrust between the open water propeller and the ducted propulsor. The r/R of the rotor is 0.470 and places the ducted inside the "knee" of the boundary layer. This judgment observation is clouded by the fact that the boundary layer diffuses over the tapered stern, and thus the radial location of the "knee" changes with axial position.

The stator has 11 blades with the leading edge tip at $x/L = 16.5094$ and $r/R = 0.5267894$. The rotor has 6 blades with its leading edge tip at $x/L = 17.1$ and $r/R = 0.470$. There is no gap between the blades and the duct. The design J_s is 1.52. The number of stator blades, the number of rotor blades and design J_s are consistent with the full stern ducted design. Figure 6-2 shows the notional geometry.
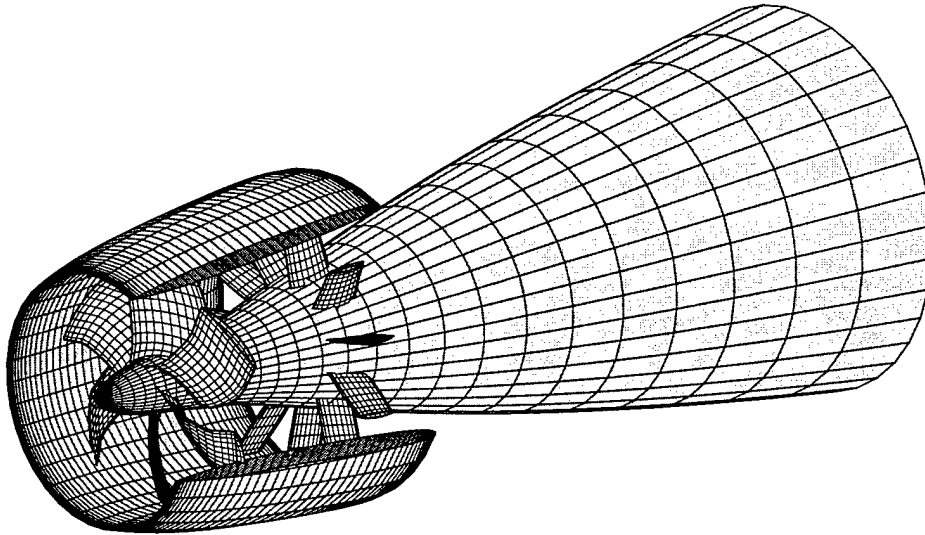

Figure 6-2: Notional tapered stern ducted design

The RANS grid models the same flow field area as the full stern grid. The grid

	Tapered with Duct
$C_{D_{SHIP}}$	0.09018
$C_{T_{SHIP}}$	0.08994
$PercentOverpowered$	-0.3
K_T	0.3694
$10 * K_Q$	0.8172
$PowerCoefficient$	0.0822
$Thrust(lbf)$	84490
$ShaftRPM$	117.4
$Torque$	245973
$MaxSpeed(knots)$	23.2

Table 6.3: Results for the ducted, tapered stern submarine.

starts at $x/L = 8.0$ and extends to $x/L = 80.0$. The number of cells is maintained similar to the number of cells in the full stern grid. Therefore, the grid resolution is very nearly identical to the full stern grid. As in the non-ducted case, the full scale corrections are shown in Table 6.1.

6.2.2 Powering Characteristics

For a counter rotating set of propeller blades in a non-contracting flow field such as behind a gradually tapered afterbody, the optimum circulation distribution is very nearly constant loading [17], [20]. The powering results are shown in Table 6.3. Just as the other cases, neither the torque nor the shaft speed have limits imposed.

When compared to the open water version, the ducted version of Variant 4 demonstrates the advantage of a ducted design. With a duct present, the Variant 4 gains 0.9 knots in maximum speed. While there are literally hundreds of variables to adjust to obtain the optimum design, this simple excursion shows clear advantages of a ducted design over a open water design. These ideas are not new, they have been discussed in countless papers and reports including [20], [29], [10], [3].

Chapter 7

Conclusion and Recommendations

7.1   Summary of Results and Conclusion

The design process followed in Chapter 2 yields an honest comparison of a full stern and a tapered stern hull envelope. The parametric arrangements, while not exact, provide a good comparison of two similar versions of the same submarine. The powering characteristics developed in Chapters 3 through 6 provide a comparison of the propulsor performance which corresponds to the submarine hull envelopes developed in Chapter 2.

The ultimate goal of this thesis is to answer the question of whether a full stern is a better hull envelope than a tapered stern. Many assumptions are made throughout this study to obtain quantifiable results. Whenever possible, the assumptions are forward looking while still realistic. The hope is to include the effects of interior arrangements on the size of the envelope. Then, using the correctly sized envelope, determine the maximum speed attainable with the same install shaft horsepower.

Starting with arrangements and ending with hydrodynamic powering calculations yield significant insight on the full stern. The results, while not conclusive, promise great potential for the full stern submarine. The two designs have marked differences in length but similar displacements and similar maximum speeds. Table 7.1 summarizes the competing designs.

The full stern has a faster maximum speed than a tapered stern. The full stern

speed is 23.5 knots which compares with a tapered stern speed of 23.2 knots. The speed difference is only 1.3 % which is well within the precision of the vortex lattice / RANS method used to analyze the powering characteristics. However, recall that the full stern is not globally optimized. Many more cases can be envisioned which may yield even better performance. Thus, the closeness in speed for such a small sampling of cases promises great benefits from a full stern submarine. Therefore, additional study should be directed towards the full stern submarine to verify this study and provide more insight on the benefits and drawbacks of a full stern submarine.

7.2   Conclusion on Arrangements

The parametrics used to arrange the submarine have limitations with the issues of stack length and with volume to area conversions. Reference [11] does preliminary arrangements of a submarine which was initially sized with the parametric arrangements and gives a conclusion on the precision of the parametrics. The final design in reference [11] shows that parametrics yielded at hull envelope of 181 feet and the preliminary arrangements yielded 178 feet. Thus, the arrangement parametrics used to size the hull envelopes give reasonable size hulls. There was, however, substantial differences in the division of volume interior of the hull envelope.

The arrangements give a hull form envelope on which to base viscous and pressure drag which the propulsor must overcome. By using consistent arrangement assumptions and parametrics, the hull envelope sizes are reasonably correct relative to each other. Consequently, the propulsor characteristic provide a solid pairwise comparison between a full stern designed submarine and a tapered stern designed submarine.

7.2.1   Need for Detailed Arrangements Study

The parametrics level of arrangements consider both the submarine weight and volume. While historically submarines have been weight limited, this study considers that future submarines may be volume limited as electronics become smaller and

Arrangements	Full Stern	Tapered Stern
LBP (ft)	199	244
Sub. Disp. ($ltons$)	2781	2837
SHP (hp)	5500	5500
D (ft)	28	28
L/D	7.1	8.7
Volume (ft^3)	104,700	106,800
Wet. Surf. (ft^2)	15,140	17,800
Vol/ Wet Surf	6.91	6.00
ER length (ft)	32.5	48
ER volume (ft^3)	17,080	22,340
Propulsive Coefficient	0.81*	0.834
Estimated Max speed ($knots$)	21.8	21.6
Stern Shape	Full Stern	Tapered
Features	PWR	PWR
	Elect Dr	Elect Dr
	Ext Motor	Ext Motor

* Note: This PC is a best estimate value which allows the speed of a full stern submarine to be estimated using traditional naval architecture scaling. It does not equal the actual PC, defined as $PC = \frac{EHP}{SHP}$, due to separation near the stern when the full stern body is towed.

Vortex Lattice / RANS	Full Stern	Tapered Stern
Body Press Drag Coefficient	0.04535	0.03307
Duct Press Drag Coefficient	-0.01952	-0.02255
Total Press Drag Coefficient	0.02583	0.01052
Body Viscous Drag Coefficient	0.06809	0.08035
Duct Viscous Drag Coefficient	0.01636	0.01319
Total Viscous Drag Coefficient	0.08445	0.09354
Stator Drag Coefficient	0.00456	0.00430
Total Model Drag Coefficient	0.11484	0.1084
Full Scale Correction	-0.01316	-0.01817
Full Scale Drag Coefficient	0.1017	0.0902
Advance Coefficient (J_S)	1.52	1.52
Thrust Coefficient (K_T)	0.2544	0.3694
Torque Coefficient (K_Q)	0.04771	0.08172
Power Coefficient (C_P)	0.0789	0.0822
Max speed ($knots$)	23.5	23.2

Table 7.1: Summary of Variant 3 and 4.

lighter. The parametric study takes the most limiting of the two conditions while recognizing that, in the end, the weights will equal the volume.

None the less, the need for a detailed study on area, volume and weight must be done to fully quantify the arrangement issues of a full stern design. Reference [11] does this on a more detailed level, but still at the preliminary design level. Until a design goes into the detailed design phase the real answer to the arrangements will remain unclear.

7.3 Hydrodynamic Optimization

7.3.1 Methodology

The full stern variant could certainly be made better through more optimization. However, the quantity of variables that exist is considerable. The conclusion must be that the final Variant 3 hydrodynamic performance is at a local optimum. Strong interaction of the stern, duct, stator and rotor make the global optimization extremely difficult.

On the other hand, the Variant 4 has relatively weak interaction of the stern, duct, stator and rotor. The stern taper allows the propulsor to be designed ignoring interactions, then superimpose the propulsor characteristics on the stern and iterate to reach the global optimum.

A comparison of the hydrodynamic performance of the two variants yield insight on the full stern performance. Figure 7-1 shows the integrated drag due to pressure and viscous influences. The full stern has a large pressure drag near the entrance to the propulsor. However, the pressure drag is recovered as the flow enters duct. As discussed in Chapter 5, the body profile and its derivatives play an important role in the recovery of the pressure drag as well as the interaction between the duct and body.
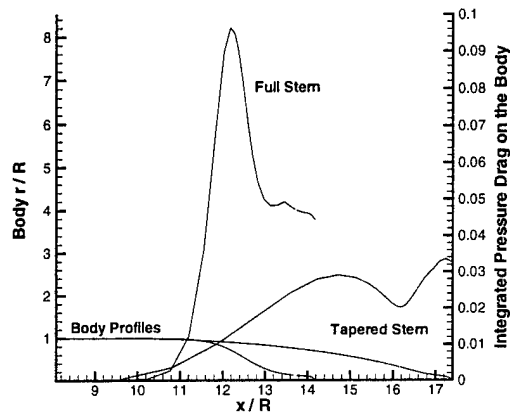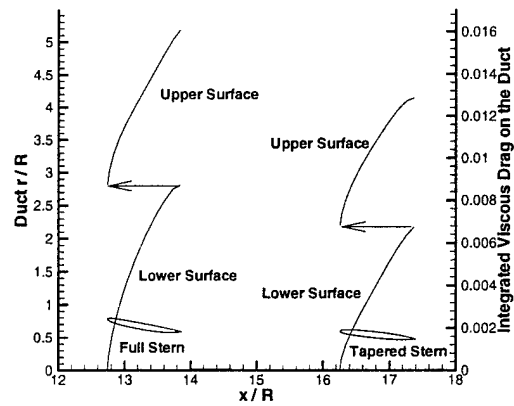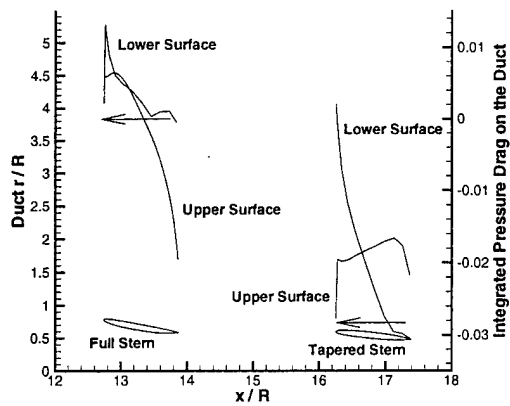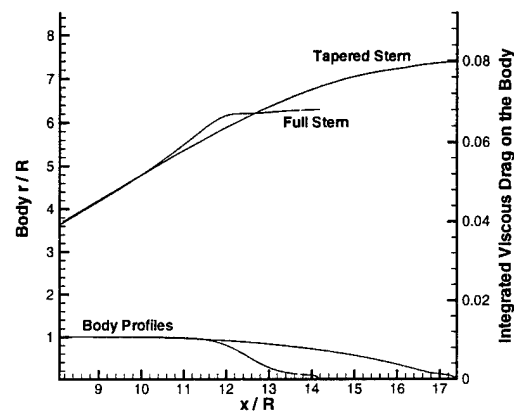
Figure 7-1: For both the full stern $(y = tanh(x))$ and ducted-tapered stern bodies, the integrated drag due to pressure and viscous influences are shown.

7.3.2 Need for Hydrodynamic Tool for Full Stern Parametric Studies

In optimizing the hydrodynamics performance of the full stern, only a limited number of cases are possible. The strong interaction of the stern components forbids a designer from optimizing one component and stating that the whole propulsor is optimized. Therefore, a design tool needs to be invented that can optimize the entire propulsor at once.

Existing blade design methods for marine propulsors, such as *PLL* developed at MIT [6], are very often based upon preliminary lifting line procedures. These

represent a propeller by a set of straight radial lifting lines and the wake as purely helical, i.e. vortices trail aft on constant radius cylinders. The limitation of these assumptions are reached since the full stern vehicles have geometries with a rapid diameter decrease at the after end. The straight radial lifting lines and helical wakes are inappropriate.

One alternate preliminary design technique which models contracted stream tubes geometries is a streamline curvature method [22]. A shortcoming of streamline curvature methods, however, is that they typically do not model the flow outside of the duct. The duct streamline is used as the outer flow boundary. Therefore, the effect of the duct is not completely included.

Work towards an improved propulsor design method is underway [27], [19], [28]. The new technique, termed *DPLL* for Ducted Propeller Lifting Line, is under development at MIT. The benefits should be significant as a typical case can be analyzed in one tenth of the time it takes now. The computational advantages include the ability to completely understand and model a full stern submarine to achieve the maximum performance.

Work should be continued on these tools and others so that the maximum performance of a full stern body can be quantified. And, if appropriate, a full stern body should be designed and built to correlate theoretical predictions with actual results.

7.3.3 Future Studies

In reviewing the methods and the results in this thesis, several ideas present themselves which may be of use in future studies. As discussed previously, the vortex lattice / RANS technique requires so much computational time that analyzing all possible cases is not practicable. By studying a carefully selected set of bodies, the powering trends can be identified in order to provide the basic data for a future full stern submarine. The following suggestions are made:

1. **Reduce Computational Time.** Use techniques that calculate less detail at the expense of accuracy. Gauge the overall trends by using more cases with less accurate methods.

2. **Full Verses Tapered Body Comparison.** When comparing a full stern design to a tapered stern design, the bodies must represent reasonable submarines. Comparisons based on equal volume are inappropriate since it may not be possible to construct a submarine within the volume constraint due to stack length issues.

3. **Quantitative Comparisons.** Performance comparisons should be based on the maximum speed for a given installed shaft horsepower. A non-dimensional quantity which represents this comparison is the power coefficient. Comparisons between a full stern and tapered stern using the propulsive coefficient are extremely misleading.

4. **Global Optimization.** Simultaneous optimization of the entire submarine, including the propulsor, is desired. However, in present day, it cannot be done. To design a full stern submarine, the ideas used in this thesis should be extended as discussed in Chapter 5. Start with a parent hull form, then meticulously examine daughter hull forms so that each daughter varies one parameter of interest.

5. **Parent Hull Form.** Chose a parent hull form which has the characteristics in the middle of the expected evaluated range. If the parent is in the middle of the range to be evaluated, then the trends developed from the daughters will likely hold.

6. **Optimization Techniques.** The parent-daughter method is analogous to a hill climber optimization technique. Other methods will work, however, no computer tool currently exist to vary the all of the propulsor characteristics which are of interest to the designer. Manual intervention is necessary to ensure a complete

sampling of characteristics.

7. **Body Parameters.** From forward to aft, the full stern submarine can be described by: nose radius, length forward (forward perpendicular to the maximum body diameter), length of parallel midbody, length aft (length from maximum diameter to the aft perpendicular), radius at shoulder, inflection radius and radius at tailcone.

8. **Duct Parameters.** The duct characteristics which may affect powering include: thickness/chord, thickness distribution, camber/chord, camber distribution, chord length, angle of attack, axial location relative to body and radius of inner surface at a reference location.

9. **Propulsor Parameters.** The parameters associated with the propulsor which may affect powering include: number of pre-swirl blades, axial location and characteristics, number of rotor blades, axial location and characteristics, and the tip clearance between the rotor and duct inner surface.

10. **Towed Verses Propelled.** In a tapered afterbody, the body can be optimized for minimal drag. The propulsor is then added and the results are close to a global optimum due to the relatively weak interaction of the propulsor components. In a full stern, which will separate without an operating propulsor, optimizing the body without an operating propulsor would yield little relevant data. Instead, the optimization analysis must include an integrated propulsor to minimize powering.

11. **Body Continuity.** A surprising result of Chapter 5 was the marked reduction in drag due to only slight afterbody changes. By designing the afterbody with smooth higher derivatives, the powering improved. To capitalize on this effect, the parent and all daughter bodies must have a smooth transition from the parallel mid-body to the propulsor.

12. **Body Description.** In order to maintain smooth bodies, it may be possible to represent the body profile as a power series or as a B-spline. The number of constraints placed on the body profile dictates the order of the curve.

13. **Computer Model To Physical Model.** Lastly, testing of a physical model should be done to provide accurate and quantifiable results which can be used to validate computer models. Once, a full stern computer model is completely validated, the full stern series can be done to optimize a full stern body with great confidence.

Bibliography

[1] Marine Propulsor. Technical Report Patent Number 5,078,628, United States Patent Office, Jan. 7, 1992.

[2] Scott D. Black. An Integrated Lifting Surface/Navier-Stokes Propulsor Design Method. Master's thesis, MIT Department of Ocean Engineering, June 1994.

[3] E. P. Bruce, W. S. Gearhart, J. R. Ross, and A. L. Treaster. The design of pump-jets for hydrodynamic propulsion. In *Fluid Mechanics, Acoustics, and Design of Turbomachinery*, pages 795–839, University Park, Pennsylvania, 1970.

[4] Roy Burcher and Louis Rydill. *Concepts in Submarine Design*. Cambridge University Press, 1994.

[5] R.M Coleman. INMESH: An Interactive Program for Numerical Grid Generation. Technical Report 85/054, DTNSRDC, August 1985.

[6] W. B. Coney. A method for the design of a class of optimum marine propulsors. Technical Report 89-6, Department of Ocean Engineering, Massachusetts Institute of Technology, August 1989. Also in PhD Thesis Form.

[7] W. B. Coney, C. Y. Hsin, and J. E. Kerwin. A vortex lattice lifting line program for single and multi-component propulsors mit pll-2 report and user's manual. Technical report, Department of Ocean Engineering, Massachusetts Institute of Technology, December 1986.

[8] Thomas B. Dade. Advanced Electric Propulsion, Power Generation and Power Distribution, pp. 83-92. Technical report, Naval Engineers Journal, March 1994.

[9] Thomas B. Dade. Advanced Electric Propulsion, in a brief "Electric Drive – Coming of Age". Technical report, Newport News Shipbuilding, Sept. 1996.

[10] C. M. H. Dai, J. J. Gorski, and H. J. Haussling. Computation of an integrated ducted propulsor/stern performance in axisymmetric flow. In *Propellers/Shafting '91 Symposium*, Virginia Beach, VA, September 1991. Ships' Machinery Committee, SNAME.

[11] Alex Desroche, Chris Trost, and Chris Warren. Advanced Concept Submarine. Technical report, MIT Department of Ocean Engineering, June, 1997.

[12] Jeffery L. Dutton. Contrarotating Electric Drive for Attack Submarines, pp. 45-49. Technical report, Naval Engineers Journal, March 1994.

[13] Glenn Cann et al. *Submarine Design Notes*. IAP Mini-course, MIT Department of Ocean Engineering, January, 1995.

[14] Norman Friedman. *Submarine Design and Development*. Naval Institute Press, 1984.

[15] W.S. Gearhart and R.E. Henderson. Selection of a propulsor for a submersible system. *Journal of Aircraft*, 3(1):84–90, 1966.

[16] J. J. Gorski. Multiple block calculations of the Navier-Stokes equations for incompressible flows. In *Proceedings of the 12th U.S.-Federal Republic of Germany Data Exchange Meeting*, Bethesda, MD USA, 1988.

[17] T. T. Huang, H. T. Wang, N. Santelli, and N. C. Groves. Propeller/stern boundary layer interaction on axisymmetric bodies : Theory and experiment. Technical Report DTNSRDC 76-0113, DTNSRDC, December 1976.

[18] J. E. Kerwin, D. P. Keenan, S. D. Black, and J. G. Diggs. A Coupled Viscous/Potential Flow Design Method for Wake-Adapted, Multi-stage, Ducted Propulsors. In *Proceedings, Society of Naval Architects and Marine Engineers*, 1994.

[19] J.E. Kerwin, S.D. Black, T.E. Taylor, and C. Warren. A Design Procedure for Marine Vehicles with Integrated Propulsors. In *Propellers/Shafting '97 Symposium*, Virginia Beach, VA, September 1997. Ships' Machinery Committee, SNAME.

[20] Justin E. Kerwin. 13.04 Lecture Notes - Hydrofoils and Propellers, February 1995.

[21] E. V. Lewis. *Principles of Naval Architecture*. SNAME, Jersey City, NJ, 1988.

[22] M. W. McBride. The design and analysis of turbomachinery in an incompressible steady flow using the streamline curvature method. Technical Report TM 79-33, The Penn. State Univ., February 1979.

[23] Capt (ret.) Harry Jackson. *Submarine Design Trends*. Draper Laboratory, Cambridge, MA, 1996.

[24] Capt (ret.) Harry Jackson. *Future Submarine*. Unpublished, December, 1995.

[25] Capt (ret.) Richard Sharpe. *Jane's Fighting Ships 1996-97*. Jane's Information Group Limited, Sentinel House, 1996.

[26] John Stenard. Comparative Naval Architecture of Modern Foreign Submarines. Master's thesis, MIT Department of Ocean Engineering, June 1988. also Naval Engineer's thesis.

[27] Todd E. Taylor. *Preliminary Design and Analysis of Propulsors for Axisymmetric Underwater Vehicles*. PhD thesis, MIT Department of Ocean Engineering, September 1996.

[28] M. W. Thomas. *Title to be decided.* PhD thesis, Massachusetts Institute of Technology, June 1998.

[29] S. Thurston and M.S. Evanbar. Efficiency of a propulsor on a body of revolution-inducting boundary-layer fluid. *Journal of Aircraft*, 3(3):270–278, 1966.

[30] Christopher Trost. Thermoelectric Reactor Submarine Trade-Off Study. Technical report, MIT Department of Ocean Engineering, July 1996.